

**BASAL BIOENERGETIC ABNORMALITIES IN SKELETAL MUSCLE FROM RYANODINE
RECEPTOR MALIGNANT HYPERTHERMIA SUSCEPTIBLE R163C KNOCK-IN MICE ***

**Cecilia Giulivi¹, Catherine Ross-Inta¹, Alicja Omanska-Klusek¹, Eleonora Napoli¹, Danielle Sakaguchi¹,
Genaro Barrientos¹, Paul D. Allen², and Isaac N. Pessah¹**

From ¹Department of Molecular Biosciences, School of Veterinary Medicine, University of California, Davis, CA 95616, and ²Department of Anesthesiology Perioperative and Pain Medicine, Brigham & Women's Hospital, Boston, MA 02115

Running head: RyR1 mutation and mitochondria

Address correspondence to: Dr. Cecilia Giulivi, University of California, Dept. VM: Molecular Biosciences, One Shields Ave, 1120 Haring Hall Davis, CA 95616; email: cgiulivi@ucdavis.edu

Malignant hyperthermia (MH) and central core disease (CCD) in humans have been associated with mutations in the skeletal ryanodine receptor (RyR1). Heterozygous mice expressing the human MH/CCD RyR1 R163C mutation exhibit MH when exposed to halothane or heat stress. Considering that many MH symptoms resemble those that could ensue from a mitochondrial dysfunction (e.g., metabolic acidosis, hyperthermia), and that MH susceptible mice or humans have a higher than normal cytoplasmic Ca²⁺ concentration at rest, we evaluated the role of mitochondria in skeletal muscle from R163C compared to wild type mice under basal (untriggered) conditions. R163C skeletal muscle exhibited a significant increase in matrix Ca²⁺, increased ROS production, lower expression of mitochondrial proteins, and higher mtDNA copy number. These changes, in conjunction with lower myoglobin and glycogen contents, Myh4 and GAPDH transcript levels, GAPDH activity, and lower glucose utilization suggested a switch to a compromised bioenergetic state characterized by both low oxidative phosphorylation and glycolysis. The shift in bioenergetic state was accompanied by a dysregulation of Ca²⁺-responsive signaling pathways regulated by calcineurin and ERK1/2. Chronically elevated resting Ca²⁺ in R163C skeletal muscle elicited the maintenance of a fast-twitch fiber program and the development of insulin resistance-like phenotype as part of a metabolic adaptation to the R163C RyR1 mutation.

Malignant hyperthermia (MH), an inherited pharmacogenetic disorder of skeletal muscle characterized by an abnormal response to muscle depolarizing muscle relaxants such as succinylcholine and volatile anesthetics (1). In some cases MH susceptibility is associated with Central Core Disease (CCD; MIM117000), a congenital myopathy defined by areas with reduced oxidative activity due to mitochondria depletion (2,3) and the presence of “central cores” within the longitudinal axis of the muscle fiber (4). CCD has a typical onset in infancy and presents with hypotonia and motor developmental delay. MH can manifest in the absence of any clinical diagnosis of CCD (1,5-8), and is one of the main causes of death due to anesthesia affecting humans, dogs, pigs, and horses (9,10). The fulminant MH episode is characterized by muscular rigidity, rhabdomyolysis, rapid increase in body temperature and signs of generalized metabolic decompensation, which can rapidly lead to death of the patient if unabated (11). MH susceptibility and CCD are allelic conditions stemming from predominantly dominant mutations in the type 1 ryanodine receptor (RYR1) gene. RYR1 encodes the skeletal muscle sarcoplasmic reticulum calcium release channel (RyR1) (12-14), and more than 178 mutations have been identified throughout the RYR1 gene to date, most of them missense mutations, with a few being deletions and splicing site mutations (15-24). A few rare mutations conferring MH susceptibility have been associated with mutations in CaV1.1, the major subunit of the sarcolemmal slow voltage gated Ca²⁺ channel (CACNA1S, dihydropyridine receptor, DHPR) (25,26).

Genotype-phenotype correlations associated with mutations in the RYR1 gene are complex, and may be partly explained by how mutations in different regions of the RyR1 protein influence conformation and functional regulation of the channel. Subtle functional differences among the large number of mutations currently known could also explain why a subset of mutations confer MH susceptibility without clinical evidence of early onset CCD, whereas others confer MH and CCD of varying severity (15,20-22,27).

Muscle fibers and myotubes isolated from knock-in mice expressing the MH/CCD RyR1 R163C mutation have augmented Ca^{2+} SR Ca^{2+} leak that leads to chronically elevated cytoplasmic Ca^{2+} (28,29), and potentiated depolarization-induced Ca^{2+} entry (30-32). Collectively these data indicate that MH mutations dramatically impact intracellular Ca^{2+} balance in resting muscle as well as alter the dynamics of bidirectional signaling during EC coupling. How these aspects of Ca^{2+} dysregulation influence respiratory parameters and mitochondrial functions in the non-triggered (basal) state is poorly understood.

More than 40 years ago, it was suggested that uncoupling of oxidative phosphorylation could explain the metabolic disturbances seen in MH (33). However, other labs were not able to show that halothane uncoupling of oxidative phosphorylation could explain the rapid rise in body temperature seen in MH (34). Furthermore, no difference was detected in isolated mitochondria from control and MH patients during halothane exposures (35,36). Most of the metabolic symptoms associated with fulminant MH episodes can be described as the result of an acute mitochondrial dysfunction secondary to abrupt loss of SR Ca^{2+} regulation. Muscle biopsies from some MH susceptible individuals show histological evidence of mitochondrial abnormalities, including clumping and presence of inclusion bodies (37-40). Studies of MH susceptible porcine skeletal muscle strips using ^{31}P NMR spectroscopy suggested that induction of anoxia in MH muscle caused significantly more rapid fall in intracellular phosphocreatine, elevation of inorganic phosphate, and diminution of ATP, compared to normal muscle (41). Non-invasive ^{31}P MRS studies have indicated that leg skeletal muscles of MH susceptible patients have higher resting PDE/PCr and Pi/PCr ratios (42,43). More recently, mitochondria were found to be swollen and misshapen from skeletal muscle of heterozygous Y522S mice (44) but no studies have been

performed to date to link any of the RyR1 mutations with changes in mitochondrial bioenergetics under basal conditions (untriggered). The current study focuses on studying metabolic differences in MH susceptible and WT skeletal muscle under basal conditions. To this end, C57BL6 WT mice and C57BL6 knock-in mice expressing the R163C-RyR1 mutation, which is one of the most common human MH mutations, were utilized in the present study (45). We investigated the effect of this RyR1 mutation on mitochondria obtained from skeletal muscle, in which the expression of full-length RyR1 is found, and its downstream Ca^{2+} -dependent effectors are tailored to suit the distinctive function of this organ.

EXPERIMENTAL PROCEDURES

Animals- All experiments on animals from creation of MH/CCD mice to establishment of their physiologic and biochemical phenotypes were conducted using protocols approved by the institutional animal care and use committees at the Australian National University, Harvard Medical School, and the University of California at Davis essentially as previously described (45). Heterozygous R163C malignant hyperthermia-susceptible (MHS) mice were generated with a knock-in mutation-targeting vector as previously described (45). Heterozygous C57BL6/129svJ R163C-RyR1 mice were back bred with congenic WT C57BL6 >10 generations and their genetic background confirmed by SNP analysis. Mitochondria for functional and biochemical analyses were isolated from 7-to-10 month-old mice killed by cervical dislocation. Where indicated, perfusion of the animals was performed by cardiac puncture with PBS supplemented with 10 mM EGTA, prior removal of skeletal muscle.

RNA Extraction and Quantitative real-time PCR (qPCR)- Total RNA was extracted from tissues using RNEasy Plus (cat no. 74134) extraction kit from Qiagen following the manufacturer's instructions. The quality and quantity of extracted RNA was performed by using the 2100 Bioanalyzer from Agilent. Reverse transcription was performed using Qiagen's Quantitect RT kit (catalog # 205311) according to the manufacturer's instructions. Transcript-specific primers and probes for MYH1 (Mm01332489_m1), MYH2 (Mm01332564_m1), MYH4 (Mm01332541_m1), MYH7 (Mm00600555_m1), GAPDH (Mm99999915_g1), ActB (Mm01205647_g1) and B2M (Mm00437764_m1) were purchased from Applied Biosystems Assays on Demand library. Real-time

PCR was done with TaqMan Universal Mastermix (Applied Biosystems) with 400 nM of each primer, 80 nM of fluorogenic TaqMan probe, and 5 nM of template at 111 ng using Mastercycler EP Realplex thermocycler (Eppendorf, Westbury, NY). Amplification was performed using the following parameters, 2 minutes at 50°C (activation of UNG enzyme), 10 minutes at 95°C (deactivation of UNG and activation of AmpliTaq Gold DNA polymerase), and 40 cycles of 15 seconds at 95°C and 60 seconds at 60°C. The mean cycle time obtained by double derivatives (CalqPlex algorithm; Eppendorf, Westbury, NY) was designated as Ct. Each sample was analyzed in triplicates. Positive and negative controls were run in each plate. The corresponding real-time PCR efficiencies for each gene amplification were calculated according to the equation: $efficiency = 10^{(-1/slope)} - 1$. After establishing the linear response between Ct number and template amount (1000, 500, 250, 125, and 62.5 ng total per reaction), efficiencies for each gene were between 95%-104%. To choose a gene to normalize our RT-PCR data and given the issues regarding selection of genes for this purpose (46,47), we tested three genes normally selected as housekeeping genes (B2M, Act5b, and GAPDH). The expression stability was determined by using three types of algorithms provided by GeNorm, NormFinder, and BestKeeper softwares (48-50). No statistical differences were found between B2M and Act5b, and both were found to be stable enough in this system to act as housekeeping genes. Linear fold difference was determined through the $2^{-\Delta Ct}$ method.

Isolation of mitochondria-The mitochondrial fraction was prepared from skeletal muscle (predominantly type II fibers mixed) in buffered mannitol-sucrose-EDTA using minor modifications of the previously described procedure (51). The mitochondria were isolated by mechanical cell disruption using a glass-Teflon homogenizer and subsequent centrifugation, followed by purification in a Percoll gradient (52,53). After cervical dislocation, where indicated, the animals were perfused with 10 mM EGTA in PBS by cardiac puncture. Muscle (brachii, hind legs) were quickly removed, immersed in cold 0.25 M sucrose, and washed until the solution came out clear of blood. All connective tissue and fat was removed, the tissues were blotted, and weighted. Then they were placed in 0.22 M mannitol, 70 mM sucrose, 0.5 mM EGTA, 2 mM HEPES, 0.1% fatty acid-free BSA, pH 7.4 (MSHE) kept at 4°C, cut in smaller pieces

with fine scissors in beakers kept on ice, and homogenized in glass-Teflon homogenizer using a 5:1 buffer to muscle wet weight ratio. The muscle was homogenized in a Polytron homogenizer (PT 2100) using a micro-attachment at 11,000 rpm using one to three 5 s bursts. Large cell debris and nuclei were pelleted by centrifuging at 600 g for 5 min in a Sorvall refrigerated centrifuge. Lipid material, which packed at the surface of the supernatant, was removed and the supernatant filtered through two layers of cheesecloth. This fraction was named total (T). Mitochondria were pelleted by centrifuging the supernatant for 10 min at 10,300 g in the same centrifuge. This pellet was called mitochondria-enriched fraction while the supernatant was the post-mitochondrial (PM) fraction. The mitochondria-enriched fraction was purified using a self-forming Percoll gradient. The pellet was suspended in 25 ml of 0.225 M mannitol, 5 mM HEPES, 1 mM EGTA, 0.1% fatty acid-free BSA, 30% Percoll, pH 7.4 at 4°C, and spun for 30 min at 95,000 g in a Beckman Ti-60 rotor at 4°C. Mitochondria were separated from microsomal, sarcoplasmic reticulum, broken mitochondria, and other contaminants located at the top layer (52,54,55). Mitochondria were collected from the second band from the top (density 1.05-1.10 g/ml), washed carefully, re-suspended in buffer MSHE using 2-4 gentle strokes with a loose-fitting pestle in a Teflon-glass homogenizer, and centrifuged 10 min at 6,300 g. This step was repeated again, and finally the pellet was washed using 0.15 M KCl. Mitochondrial pellets were gently suspended in a small volume of ice-cold buffer MSHE supplemented with protease and phosphatase inhibitors (at a 1:100 V/V dilution; Sigma catalog # P8340, P2850 and P5726) to give a final protein concentration of 7-10 mg/ml. All oxygen consumption studies were immediately performed, whereas aliquots of mitochondria and PM fractions were stored at -80°C for further enzymatic analyses and protein evaluation. Protein was determined by the BCA protein assay (56) using a commercially available kit from Pierce.

Mitochondrial oxygen consumption -Mitochondrial oxygen consumption was measured using previously described methods (51). All measurements were completed in at least duplicates using mitochondria (0.5-1 mg/ml) in 0.22 M sucrose, 50 mM KCl, 5 mM MgCl₂, 1 mM EGTA, 10 mM KH₂PO₄, 10 mM HEPES pH 7.4 (reaction buffer). Briefly, an aliquot of mitochondria were added to the oxygen chamber that contained 1-ml of

reaction buffer (final protein concentration 0.5-1 mg/ml). The oxygen uptake was measured using a Clark-type O₂ electrode from Hansatech (King's Lynn, UK) at 22°C using constant stirring. Oxygen consumption rates were evaluated in the presence of buffered 1 mM malate-10 mM glutamate followed by the addition of 1 mM ADP to record State 3 oxygen uptake. Then, 5-μM rotenone was added, followed by the addition of 10 mM succinate. This oxygen consumption was inhibited by adding 3.6 μM antimycin A. Cytochrome *c* oxidase activity was evaluated as the (1 mM KCN) KCN-sensitive oxygen uptake in the presence of 10 mM ascorbate and 0.2 mM *N, N, N', N'*-tetramethy-*p*-phenylenediamine (TMPD). State 3 respiration is defined as the oxygen consumption rate in the presence of 1 mM malate-10 mM glutamate and 1 mM ADP. State 4 oxygen consumption was determined in the presence of maximal amounts oligomycin (8 μg/mg mitochondrial protein), a specific inhibitor of the ATP synthase. ATP synthase inhibition was confirmed by determining if addition of oligomycin caused further inhibition of oxygen consumption.

Muscle oxygen consumption- Immediately after muscle isolation, hind leg muscles were sectioned and permeabilized for 30 min as described (57). All procedures were performed in a cooling room on ice at 4°C. Oxygen consumption was performed using the same apparatus described above in the presence of 10 mM NADH and 1 μM FCCP in reaction buffer, followed by the inhibition with rotenone or antimycin. Where indicated, mouse diaphragm was excised and prepared for glucose and oxygen uptake as described by (58) with the following modifications: (30 to 45 mg of wet weight) muscle was placed in the oxygen chamber using the apparatus described above in buffered modified Ringer solution with 10 mM glucose at 22°C, followed by the sequential addition of the following chemicals separated by 5-8 min intervals (enough to detect a significant rate): 5 μg/ml oligomycin, 5 nM FCCP, and 5 μM rotenone; triplicate aliquots were taken at time zero and at 2.5 hours to evaluate glucose and lactate. These compounds were determined using an YSI 2300 STAT Plus glucose analyzer (YSI Life Sciences, Yellow Springs, OH).

Calcium concentrations- Water used throughout was obtained from a MilliQ water purification system at a resistivity of 18 MΩ.cm. Nitric acid (puriss. p.a.) was from Sigma (< 3 x 10⁻³ ppm in calcium). Total mitochondrial and cytosolic calcium concentrations were determined by

inductively coupled plasma mass spectrometry at the University of California Davis, Interdisciplinary Center for Plasma Mass Spectrometry. Briefly, the samples were diluted to 1 mg protein/ml in 3% nitric acid, filtered to eliminate particulate matter, and digested for 6 h at 90 °C. Upon cooling, the samples were submitted to the Facility. Blanks contained less than 10 nM calcium, 100-fold lower than the calcium concentration obtained with whole muscle tissue (~1 μmol/g wet weight).

Complex activities- Complex I activity was evaluated by following the NADH-CoQ₀ oxidoreductase activity (NQR) was evaluated according to (59) with the following modifications. The assay was measured at 340 nm following the oxidation of NADH at 37°C. In 160 μl of water, 5-μg of cell protein was added and incubated for 2 min at 37°C. Then, 50 μl of buffer containing 5 mg/ml BSA, 240 μM KCN, 4 μM antimycin A, 40 mM HEPES/KOH, pH 7.5 were added. The reaction was started with the addition of 50 μM 2,3-dimethoxy-5-methyl-1,4-benzoquinone (or CoQ₀). The absorbance changes were followed in a Molecular Devices Spectramax M2 plate reader using the Soft Max Pro software version 4.7.1. Data points were taken every 34 seconds for 10 minutes. Five-μM rotenone was then added and the reaction was followed for an additional 5 min. Rotenone-sensitive activities were calculated from the linear part of ΔA vs. time plots and using an extinction coefficient of 6.22 mM⁻¹ cm⁻¹. Succinate-cytochrome *c* reductase (SCCR), which evaluates Complex II-III, and cytochrome *c* oxidase (Complex IV) activities were evaluated as described by (59) but performed in a microplate reader (2-8 μg protein/well and all reagents were scaled down from 1-ml to 0.2 ml). Complex II activity was measured by following the reduction of 2,6-dichlorophenolindophenol at 600 nm. The reaction was carried out with succinate, in the presence of KCN and rotenone and initiated by the addition of ubiquinone-2. The rate sensitive to 2-thenyltrifluoroacetone (1 mM) was taken as Complex II activity (60). Complex V was evaluated by following ATPase activity (61). The assay was performed at 340 nm following the reduction of NADH. Each well contained 2-8μg of protein, 140 μl of reaction buffer (in mM; 1.5 phospho(enol) pyruvate, 0.25 NADH, 45 MgCl₂ and 45 HEPES, 6.3 units/ml pyruvate kinase and 4.5 units/ml lactic dehydrogenase pH 7.5). The reaction was started with the addition of 2 mM ATP and followed for 5 min. Then, 5 μg/ml of oligomycin was added and

the reaction was followed for an additional 5 min. The rates were followed at 37°C in a SpectraMax microplate reader. The oligomycin-sensitive rate was expressed as nmol ATP hydrolyzed/min mg protein.

Citrate synthase activity-This activity was evaluated in isolated mitochondria by spectrophotometry (59). Isolated mitochondria were diluted to a final concentration 1 mg protein/ml in 20 mM HEPES, pH 7.4 on ice, and homogenized for 30 s. The assay was performed at 412 nm following the reduction of 0.1 mM 5,5'-dithiobis (2-nitrobenzoic acid) in the presence of 5–30 µg of homogenized mitochondria, 0.2 mM acetyl-CoA in a medium with 10 mM Tris-HCl, pH 8.1, and 0.2% Triton X-100. The reaction was started by adding 0.5 mM oxalacetic acid. The rates were calculated from the linear part of $\Delta A/\text{min}$ vs. mg protein plots and using an extinction coefficient of $11,400 \text{ (M} \times \text{cm)}^{-1}$.

Glyceraldehyde-3-phosphate dehydrogenase (GAPDH) activity- GAPDH activity was measured with a kit purchased from Biomedical Research Service Center (BRSC, Buffalo, NY, USA). The colorimetric assay is based on the reduction of idonitrotetrazolium to formazan in an NADH-coupled enzymatic reaction using glyceraldehyde-3-phosphate as substrate (62). Briefly, 3 to 5 µg of skeletal muscle proteins were diluted 1:1 with 2X cell lysis solution and added to a 96-well microplate. Ten-µl of 1X cell lysis solution were used as blank. The enzymatic reaction was initiated by adding 50 µl of the GAPDH Assay Solution to each well and the formation of formazan was monitored at 492 nm for 45 min at 37 °C. The reaction exhibited a linear range for the whole duration of the assay and the specific GAPDH activity was expressed as nmol formazan formed \times (min \times mg protein)⁻¹ using an extinction coefficient of $19,900 \text{ (M} \times \text{cm)}^{-1}$.

ROS production- The rate of H₂O₂ production in mitochondrial preparations was followed fluorometrically using 5 U/ml horseradish peroxidase (HRP) coupled to 40 µ M *p*-hydroxyphenylacetic acid oxidation (63). Succinate (10 mM), in the presence of 5-µM rotenone and 3.6-µM antimycin, was used as substrate for this assay. Mitochondria lysate (0.5-0.6 mg/assay) were added to start the reaction. Increased fluorescence at 22°C was monitored by a Shimadzu fluorimeter. Arbitrary fluorescence units per minute for the reaction were converted to amount of H₂O₂ by

comparing the values to a standard curve generated over a range of H₂O₂ concentrations. H₂O₂ generation was expressed as nmol H₂O₂/min/mg protein. The addition of selective inhibitors of the respiratory chain permitted delineation of sites of mitochondrial ROS production.

Evaluation of mtDNA copy number- The mtDNA copy number was evaluated by the mtDNA/nDNA ratio. To this end, quantitative real-time PCR (qTPCR) with dual-labeled probes was performed on genomic DNA. The targeted genes were the single-copy nuclear PK and mitochondrial CYTB, ND1, ND4 and ND2. Species-specific primers were selected using the Primer Express 3 software (Applied Biosystems). Mouse primers for PK were: forward 5'-CCCAGACAACCTACATACCAGCTAATC-3'; reverse 5'-CTCCATCAACAAGCCGAAAAG-3'; fluorogenic probe used was UPL #6 (Roche Universal Probe Library). Primers for CYTB were: forward 5'-CCCAGACAACCTACATACCAGCTAATC-3'; reverse 5'-AGGCTAGGACACCTCCTAGTTTATTG-3', BHQ-FAM labeled probe from Operon was 5'-TAAACACCCACCCCATATTAACCCGAA-3'. ND4 primers were: forward 5'-ATCACTCCTATTCTGCCTAGCAAAC-3'; reverse 5'-AAGTCCTCGGGCCATGATTA-3' and BHQ-FAM labeled probe from Operon was 5'-CCAACCTACGAACGGATCCACAGCCGTA-3'. ND1 primers were: forward 5'-CAAACACTTATTACAACCCAAGAACAC-3'; reverse 5'-AATCATATTATGGCTATGGGTCAGG-3' and UPL #29 was used from Roche. ND2 primers were: forward 5'-CACGATCAACTGAAGCAGCAAC-3'; reverse 5'-GTACGATGGCCAGGAGGATAAT-3' and UPL #90 was used from Roche. The corresponding real-time PCR efficiencies for each mitochondrial and nuclear gene amplification were calculated according to the equation: $E = 10^{(-1/\text{slope})} - 1$. After establishing the linear response between Ct number and template amount (25, 12.5, 6.25, 3.13 and 1.56 ng total per reaction), efficiencies for each gene were between 95%-100%. Genomic DNA was extracted from cell cultures using Puregene kit from Qiagen. DNA concentrations were determined by using Thermo Scientific's nanodrop. DNA was diluted to 0.626 ng/µl and served as stock DNA template for qPCR. qPCR was performed in a Mastercycler EP Realplex thermocycler (Eppendorf,

Westbury, NY) with 7 μ l of master mixture (TaqMan 2x PCR Master Mix; Applied Biosystems with 400 nM of primers and 80 nM of fluorogenic probes) and 5 μ l of 3.13ng total of template were used per reaction. Amplification was performed using the default cycling parameters: 2 minutes at 50°C (activation of UNG enzyme), 95°C for 10 min (AmpliTaq Gold activation), followed by 40 cycles of 15 seconds of cycled denaturation at 95°C, 60 seconds and annealing/extension at 60°C. The mean cycle time obtained by double derivatives (CalqPlex algorithm; Eppendorf, Westbury, NY) was designated as Ct. Relative mtDNA/nDNA was assessed by a comparative Ct method, using the following equation: $\text{mtDNA/nDNA} = 2^{-\Delta\text{Ct}}$, where $\Delta\text{Ct} = \text{Ct}_{\text{mitochondrial}} - \text{Ct}_{\text{nuclear}}$. Each sample was analyzed in triplicates. Positive and negative controls were run in each plate. mtDNA deletions were considered if the ND4/ND1 and CYTB/ND1 ratios were lower than the mean ratio of TD – 2.58 x SD (standard deviation), or in other words, at the lowest limit of a 99% confidence interval (64). To obtain absolute gene copy number ratios, synthetic genes were ordered through Operon by providing the company with the sequences of amplicons of interest. The synthetic amplicons were cloned into pCR2.1 vector – confirming the final product through sequencing. The molecules per microliter were calculated using the following formula: $\text{Molecules } /\mu\text{l} = \text{Avogadro number} \times \text{concentration (g}/\mu\text{l)} \times (\text{Molecular weight (g/mol)})^{-1}$; where Molecular weight is equal to the total number of base pairs in plasmid plus the number of bases in inserted amplicon multiplied by 660 g/mol bp. The purified plasmid was then normalized to 2×10^9 molecules/ μ l and served as a stock solution. To generate standard curves a series of eleven ten-fold dilutions were made. The assays were run beginning from total of 1×10^7 molecules per well. All reactions were performed in triplicates to establish the linear response between the Ct values and the log of known copy numbers. The copy numbers for each samples were calculated using the equation $y = mx + b$, where y = raw Ct value, m = slope from the plasmid curve, x = the log of copy numbers, b = the y intercept of the plasmid curve.

Glycogen and triglyceride contents in skeletal muscle- Muscles were harvested from euthanized mice, freeze-clamped in liquid nitrogen, and stored at –80°C for later analysis. Glycogen content was evaluated essentially as described by (65). For total lipid content, frozen pieces of tissue were homogenized with Folch reagent (66). The organic

layer was dried under a nitrogen stream, and the lipid remaining on evaporation was weighted and evaluated by enzymatic analysis using a commercially available kit from BioVision (catalog number K622-100).

Western blotting- Proteins were denatured in SDS-PAGE sample buffer (BioRad) plus 1.5% DTT at 100°C for 3 min. Two to ten μ g of protein (or 10 – 40 μ g for nitrotyrosine) were loaded onto a 4-15% gradient SDS-PAGE gel (BioRad) and electrophoresed at 150V, 4°C for approximately 60 min. Proteins were transferred via semi-dry transfer (20% methanol, 0.0375% SDS except for nitrotyrosine blots, in which no methanol or SDS was utilized) to a 0.45 μ m PVDF membrane for 30 min at 15 V, 300 mA) Membranes were washed once for 5 min in Tris buffered saline plus tween-20 (TBST; 150 mM NaCl, 25 mM Tris, pH 7.4, 0.1% tween-20), blocked for 1 h with 5% nonfat dry milk in TBST. For nitrotyrosine blots, the blocking buffer was constituted by 1% nonfat dry milk, 1% bovine serum albumin, 10% goat serum in TBST. The nitrotyrosine blots were blocked for 2 h at room temperature. Membranes were incubated overnight at 4°C (or 48 h at 4°C for nitrotyrosine blots) with the primary antibody (**Supplementary Table I**). Membranes were washed 3 x for 5 min in TBST and then incubated with the secondary antibody conjugated to HRP. Membranes were washed 3 x for 10 min in TBST, once for 5 min in TBS and visualized with chemiluminescent reagents on a Kodak 2000MM Imager or LiCor Imager for RyR1. Images were analyzed with the software provided by the manufacturer.

*Data and Statistical analyses-*The DAVID gene functional classification tool (67,68) was used to condense the list of genes/proteins detected in our sample set into functionally related groups. We used the novel agglomeration method to cluster the three main gene ontology charts (Biological Process, Molecular Function and Cellular Component) in a meaningful network context. Student's *t*-test was used to compare data between two groups. One-way ANOVA and the Bonferroni correction were used to compare data between three or more groups. Values were expressed as mean \pm SEM. Values with $p \leq 0.05$ were considered statistically significant.

RESULTS

Similar RyR1 protein expression in skeletal preparations from wild type (WT) and R163C mice

To ensure that the genetically modified mice had the same level of RyR1 protein as WT, protein

expression was evaluated by western blot analysis of whole skeletal muscle membranes using monoclonal antibody 34C that selectively recognizes mouse RyR1 over RyR2 by western blotting (69). No significant differences in RyR1 expression were detected between WT and R163C skeletal muscles (**Figure 1 A and B**). Moreover, western blotting of RyR1 levels in the mitochondrial (M) and post-mitochondrial (PM) fractions prepared from WT and R163C skeletal muscle used to study bioenergetics were not significantly different (data not shown). Collectively these data indicate that any changes observed in R163C mice have to be attributed to the RyR1 missense mutation and not to altered expression of protein levels.

Lower State 3-dependent oxygen uptake rates in RyR1 R163C skeletal muscle mitochondria

The mitochondrial fraction was prepared from skeletal muscle (predominantly type II fibers mixed) in buffered mannitol-sucrose-EDTA by differential centrifugation, followed by purification in a Percoll gradient. Our procedure resulted in preparations of relatively high yield, similar to those published by other laboratories for WT muscle; however, the mitochondrial mass (evaluated by the mg mitochondrial protein *per g* of tissue wet weight) of R163C muscle was 61% of WT (**Table I**). The most important criteria of membrane integrity and coupling between electron transfer and ATP synthesis are the respiratory control ratio (rate of oxygen utilization in State 3 under phosphorylating conditions divided by the rate in State 4 or non-phosphorylating conditions; (70,71)) along with the P/O ratio (dependence of oxygen utilization on the availability of ADP (72)). Skeletal muscle mitochondria isolated from WT mice consistently showed relatively high RCR values (6.1 ± 0.7 ; **Table I**) comparable or higher to literature values using a wide range of techniques in various species (**Table I**). Similarly, the P/O values (2.3 ± 0.1) were in the range of those reported before (**Table I**). Although P/O values measured with R163C mitochondria did not differ from WT, the majority of R163C mitochondria were uncoupled when compared to controls (88%; RCR = 1.6 ± 0.3 ; $p < 0.05$; **Table I**).

Purified skeletal muscle mitochondria from WT and R163C mice consumed oxygen in the presence of NAD-linked (malate-glutamate) or FAD-linked (succinate) substrates when supplemented with ADP (State 3-dependent oxygen uptake rate; **Table II**). State 3 respiration rate is the

rate measured where all required substrates are present in excess and the respiratory chain itself is the rate-limiting factor; that is, the state of "active" respiration. The rates of oxygen uptake by R163C skeletal muscle mitochondria relative to WT were $62 \pm 3\%$ with an NAD-linked substrate (malate-glutamate) and $32 \pm 3\%$ with an FAD-linked substrate (succinate; **Table II**). To discern between mitochondrial dysfunction and a simple decrease in mitochondrial number, the rates of oxygen uptake in State 3 were normalized to the activity of citrate synthase (73) due to its tight correlation with morphometric data (74,75). The rates of oxygen uptake in State 3 from R163C were more pronounced when normalized to citrate synthase activity (NADH oxidase $40 \pm 3\%$ of WT values; succinate oxidase $21 \pm 2\%$; **Table II**).

Mitochondrial dysfunction in permeabilized R163C skeletal muscle

Permeabilized skeletal muscle from R163C supplemented with NADH indicated that the maximal oxygen uptake (oxygen uptake with FCCP sensitive to rotenone inhibition) was $52 \pm 9\%$ of WT (16 ± 4 and 8.2 ± 0.5 nmol oxygen consumed (min x mg protein)⁻¹; $p = 0.05$), similar to the values obtained with isolated mitochondria supplemented with an NAD-linked substrate (**Table II**).

Mitochondrial dysfunction in intact R163C diaphragm

To evaluate mitochondrial dysfunction in a more intact biological system, the glucose uptake sensitive (associated with OXPHOS) and resistant (associated with all other glucose consumption) to oligomycin was evaluated in intact diaphragm muscles from WT and R163C mice (**Table III**). The oligomycin-sensitive glucose uptake was 3-times lower in R163C muscle than WT (**Table III**). The lower glucose consumption by OXPHOS suggested that either there was a mitochondrial dysfunction *in situ* or that the total glucose uptake was lower, proportionally decreasing the amount of glucose available to OXPHOS. Although the total glucose uptake was 20% lower in R163C muscle than WT, it could not account for the lower utilization of glucose by OXPHOS (3-fold lower; **Table III**). In R163C, the lower OXPHOS was accompanied by a relative increase in the amount of glucose utilized to produce lactate (11% higher; **Table III**). Based on these experimental data, it was possible to calculate the amount of ATP produced by OXPHOS and anaerobic glycolysis. In

R163C muscle, there was a significant decline in the total amount of ATP produced (about 50%) mainly caused by the lower amount provided by OXPHOS (39% of WT), which was not compensated by anaerobic glycolysis (only 10% higher) as expected from a Pasteur effect.

Higher mitochondrial calcium in RyR1 R163C skeletal muscle is not the direct cause for mitochondrial dysfunction

A consistent observation in the MHS myotubes (28,30,45), skeletal muscle myoballs (76), and intact skeletal muscle from several species (76-78) is that all have a chronic elevation in their intracellular steady-state calcium concentration. Given that exposure of mitochondria to a sustained higher calcium concentration may lead to higher calcium uptake and net calcium accumulation, dissipation of the electrochemical gradient, decrease ATP production, and/or organelle swelling or bursting (79-81), the calcium concentrations in mitochondrial (M) M and post-mitochondrial (PM) fractions were evaluated in WT and R163C skeletal muscle by ICP-MS. The values for total calcium contents of WT were within those reported for rodent skeletal muscle using ICP-MS or other techniques (690 to 1500 nmol/g muscle wet weight; (82-86). Skeletal muscle mitochondria from R163C mice had 5.7-times more Ca^{2+} than WT, and the Ca^{2+} concentration in the cytosolic fraction was 1.8-fold higher than WT (**Table IV**). The concentrations of PM calcium in R163C are consistent with the higher (2-4-fold) resting intracellular Ca^{2+} concentrations in intact MHS skeletal muscle from various species (76-78), and indirectly, with the presence of swollen mitochondria in skeletal muscle from aged Y522S MH mice (44) and mitochondria loss in CCD skeletal muscle fibers (2). These results indicated that skeletal muscle mitochondria from R163C-RyR1 mice have accumulated more calcium than controls under basal conditions (i.e, in the absence of a fulminant MH episode). Considering that a subpopulation of mitochondria has been found closely attached to SR (87,88), and these mitochondria are exposed to higher local resting Ca^{2+} concentration in skeletal muscle (89,90), it is likely that our calcium values represent an underestimation of the actual calcium concentrations that could be found in mitochondria closely associated with SR (90).

If the overload of calcium were the main defect in the R163C mitochondria, then perfusion of animals with EGTA (91) prior to the removal of

muscle, should restore (improve) the oxygen uptake rates of R163C mitochondria relative to WT. However, EGTA at concentrations high enough to chelate most, if not all, free Ca^{2+} , did not significantly change (10-to-30%) the State 3 rates of oxygen uptake of skeletal muscle mitochondria isolated from either WT or R163C mice. Rather it improved the coupling between electron transport and ATP synthesis in R163C mitochondria. The RCR of WT skeletal muscle mitochondria (before or after perfusion) was unchanged whereas the RCR for R163C improved 2-fold (from 1.6 ± 0.3 to 3.4 ± 0.9 ; $p < 0.05$; **Table I**). Although the RCR was partially restored after chelating labile calcium, the majority of R163C skeletal muscle mitochondria (53%) were still uncoupled under basal conditions. The partial improvement on the RCR after EGTA treatment was due to a decrease in State 4 oxygen uptake rate (53 ± 13 % loss) with no change in State 3 oxygen uptake rate indicating that calcium overload was not the direct/main cause for the relatively low State 3-dependent oxygen uptake rate in R163C skeletal muscle.

Lower activities of mtDNA-encoded Complexes in R163C skeletal muscle

Considering that the State 3-dependent oxygen uptake rates obtained with NAD- and FAD-linked substrates (**Table II**) did not allow us to discriminate what Complexes were affected in R163C skeletal muscle mitochondria, the specific activities of each Complex (Complexes I-V) was individually assessed (**Table V**). Complex I ($34 \pm 15\%$ of WT), Complex III ($68 \pm 3\%$), and Complex IV ($50 \pm 3\%$) in R163C were significantly lower than WT, but not Complex II or V (**Table V**). The relative activities of the respiratory chain Complexes are consistently conserved in functional mitochondria because a tight balance between respiratory chain activities is required to allow oxidation of various substrates. The ratios of Complex activities normalized to Complex II activities were (in average) 3-fold lower in R163C than WT for Complex I, III, and IV. These results indicated that the oxidation of both NAD- and FAD-linked substrates (i.e., fatty acids and glucose) would be altered in R163C skeletal muscle.

Complex II is the only one in the electron transport chain with all subunits encoded by the nDNA. Thus, we proceeded to test the hypothesis that the changes in mitochondrial activities observed in R163C skeletal muscle mitochondria might be attributed to defects at the transcriptional or

translational levels. Western blots probing for mitochondrial proteins encoded by either nuclear DNA (Complex II 70-kDa subunit, Mn-superoxide dismutase, voltage-dependent anion channel-1, ATPase beta-subunit, cytochrome *c*) or mitochondrial (cytochrome *c* oxidase subunits I and II, NADH-dehydrogenase subunits 1 and 6) DNA (normalized to equal total cellular protein) were (in average) 63% of WT values (**Figure 2A**). However, when the expression levels were stratified into nDNA- or mtDNA-encoded, a 2-fold difference was apparent ($81 \pm 8\%$ and $41 \pm 5\%$ for nDNA and mtDNA-encoded proteins; $p = 0.007$). These results obtained with protein expression levels matched those obtained with Complex activities (activities of Complexes encoded by both genomes were 50% lower than that encoded solely by nDNA; **Table V**) suggesting that there is a mitochondrial defect at the translational or transcriptional levels.

It has been proposed that variations in expression of mitochondrial genes in striated muscle are determined predominately by gene dosage, rather than by modulation of transcriptional efficiency (74,92-94). In some cases, over-replication of mtDNA aids with the normalization of mRNA levels of deleted genes as well as those non-deleted (74). Consistent with this view, the mtDNA copy number in R163C was 1.34-fold higher in R163C than in WT (mtDNA copy number: $3,064 \pm 39$ and $4,102 \pm 149$; $p = 0.002$), whereas the mRNA levels of three mitochondrial genes (CYTB, CCO II, and ND1) and two nuclear genes (ATPase beta-subunit and mitochondrial ribosomal protein L10), all encoding for mitochondrial proteins, were, on average, not significantly different from WT values (**Figure 2B**). These data supports the notion that R163C in muscle elicits an adaptation consistent with defects in mitochondrial number and function.

Calcineurin-initiated pathway is modulated in R163C skeletal muscle

We further tested the hypothesis that the lower OXPHOS capacity of R163C skeletal muscle originated from a calcium-dependent activation of a switch to a fast-fiber type. This would entail the specific downregulation of slow fiber-specific genes controlled by the calcineurin (Cn) pathway in skeletal muscle (95-97). The expression of Cn protein in MH muscle, estimated by western blots, was $47 \pm 15\%$ of that of controls (**Figure 3**). The expression of RCAN3 (but not that of RCAN1) when normalized to the expression of Cn was 2-to-3 fold higher in R163C skeletal muscle, when

compared to WT (**Figure 3**).

The following results were consistent with a RCAN-mediated inhibition of the Cn: (a) lower OXPHOS capacity in isolated mitochondria and in permeabilized skeletal muscle; (b) lower expression of PGC1- α protein (20% of controls; $p < 0.05$); (c) lower glycogen content (35% of the WT value; 7 ± 5 and 20 ± 9 μmol glycogen/g muscle wet weight; $p = 0.018$), both contents consistent with muscles mainly constituted by fast-twitch fibers (and in both cases, mainly by *Myh4*; **Figure 4B**); and (d) lower expression of myoglobin protein ($21 \pm 10\%$; $p < 0.05$; **Figure 3**).

However, other experimental data did not support the slow to fast-twitch fiber transition, expected from the sole and complete inhibition of the Cn-mediated pathway. First, lower mean expression of all *Myh* transcripts was observed in R163C muscle ($54 \pm 11\%$ of WT; **Figure 4A**) with significantly lower gene expression of isoforms *Myh7* (30% of WT), *Myh2* (49% of WT), and *Myh4* (51% of WT; **Table VI**) indicating that R163C muscle was still mainly constituted by fast-twitch fibers as in the WT (99.9%). The only difference was attributed to the higher contribution of type IIX/D at the expense of IIB and IIA fibers. Second, higher triglyceride deposits were observed in R163C muscle (1.5-fold of WT; 91 ± 15 and 140 ± 7 mg triglyceride/g tissue for WT and R163C; $p = 0.05$), opposite to the expectation of a slow (in which the major fuel storage is fat) to fast-twitch (in which the major fuel storage is glycogen) transition but consistent with a lower OXPHOS capacity. Consistent with a lower oxidation of fatty acids in R163C, the pACC2/ACC2 and pAMPK/AMPK were $15 \pm 12\%$ and $32 \pm 12\%$ of WT values indicating that β -oxidation of fatty acids was disfavored in R163C muscle (**Figure 3**). Third, decreased glycolytic capacity was observed in R163C muscle based on the lower transcript level of GAPDH normalized to actin ($54 \pm 2\%$ of WT; 27.4 ± 0.4 and 14.8 ± 0.7 ; $p = 10^{-4}$), lower GAPDH activity ($41 \pm 1\%$ of WT; 177.1 ± 0.6 and 73 ± 2 nmol x (min x mg protein) $^{-1}$), and less glucose consumed by intact muscle (20% decrease; **Table III**).

Other calcium-activated pathways contribute minimally to metabolic changes in skeletal muscle

Several pathways can be activated by calcium in skeletal muscle in addition to the Cn already explored above. Among them calcium/calmodulin-dependent protein kinases (CaMKs) and protein kinase Cs (PKC alpha, beta,

and gamma activated by calcium and DAG).

The involvement of CaMK family does not seem critical because their activation results in a cascade of signals that results in cell proliferation (hypertrophy; (98)) and activation of AMPK (99). The brachii muscle weight-to-body weight ratio was not significantly different between WT and R163C mice in the range of 7 to 10 months old, indicating no skeletal muscle hypertrophy (data not shown), and a relatively lower activation of AMPK was observed in R163C mice, as indicated above (**Figure 3**).

The PKC family expression and phosphorylation was studied by western blotting (**Figure 3**). No differences between WT and R163C muscles were observed in expression of total PKCs when probed with a pan-PKC antibody (not shown). In addition, no expression of phosphorylated PKC λ , β II, ζ , θ , and μ (PKD) was apparent (not shown). However, R163C preparations had levels of phosphorylated PKC ϵ (at Ser 660) and α (at Thr 638/641) that were $43 \pm 12\%$ and $58 \pm 15\%$ that measured in WT preparations ($p < 0.05$). Lower levels of active PKC ϵ might prevent the known PKC ϵ -mediated enhanced energy production and glucose uptake (100) by proteins whose functions influence directly ATP production on multiple levels (e.g., numerous glycolytic enzymes such as glyceraldehyde-3-phosphate dehydrogenase and enolase, specific subunits of various citric acid cycle enzymes such as isocitrate dehydrogenase and succinate dehydrogenase, and proteins related to mitochondrial metabolism, including the adenine nucleotide transporters and VDAC (101). Although lower activities of GAPDH were observed (see before), no significant changes in Complex II activity were obtained (succinate dehydrogenase; **Table V**) or VDAC protein expression (**Figure 2A**) thus, minimizing the role of PKC ϵ in R163C skeletal muscle.

Increased oxidative stress in R163 skeletal muscle

Dysfunctional mitochondria with impaired OXPHOS could be accompanied by an increased production of ROS (102). A 3-fold increase in ROS production by Complex III was found in R163C skeletal muscle mitochondria when compared to WT (**Table VII**). These significant differences indicated an increased cellular oxidative stress.

The Y522S MHS mutation causes calcium leak and increased the S-nitrosation of the mutant RyR1. This post-translational modification increases its temperature sensitivity for activation,

producing muscle contractures upon exposure to elevated temperatures (44). Although increased ROS production were observed in skeletal muscle from R163C mice, a lower rate of nitric oxide production was found (not shown), consistent with the lack of activation of eNOS by AMPK. In addition, western blots for nitrotyrosine (a stable and hallmark of protein modification by reactive nitrogen and oxygen species), showed no statistical change in protein C-nitration in R163C skeletal muscle proteins ($110 \pm 27\%$ of WT). Thus, in R163C MHS model, it seems unlikely that S-nitrosation of RyR1 plays a significant role for the biochemical changes observed in R163C mice.

It has been reported that increased oxidative stress increases phosphorylation and activation of ERK1/2 in various cellular settings (103-106). In other studies, it has been found that ERK1/2 activity was more than 2-fold higher in high glycolytic fast-twitch fibers than in slow-twitch fibers (107), suggesting that ERK1/2 pathway may play an important role for maintaining the high glycolytic fast-twitch fiber phenotype (108), independently of the ROS level of that particular fiber type. In our experimental model, pERK1/2 in R163C skeletal muscle was significantly activated (phosphorylated) to 300-to-500% of WT values (**Figure 3**; $p < 0.05$). Consistent with previous reports, the increases in ERK phosphorylation could be attributed to increased oxidative stress in R163C muscle, sustaining the fast-twitch fiber program.

DISCUSSION

Contraction of skeletal muscle depends on rises of intracellular Ca^{2+} concentration, which are initiated by the action potential. Myoplasmic Ca^{2+} can vary from $0.12 \mu\text{M}$ under resting conditions to as much as $1 \mu\text{M}$ during contraction or $10 \mu\text{M}$ in contractures (109). Considering that the R163C RyR1 mutation in skeletal muscle resulted in a significantly increased cytosolic Ca^{2+} (about 2-fold of the normal resting concentration, this study and (30), an activation of several calcium-dependent pathways was expected leading to the activation of a slow-twitch fiber program to increase the resistance to fatigue, the oxidative capacity, and the calcium buffering capacity of mitochondria. The values for total calcium contents of WT mitochondria evaluated in the present study were within the range of those previously reported for rodent skeletal muscle using ICP-MS or other techniques (82-86). The significantly higher concentrations of mitochondrial calcium content in R163C reported

here may stem from the chronically elevated (2- to 4-fold) resting intracellular Ca^{2+} concentrations in intact MHS skeletal muscle from various species (76-78). Our results indicate that skeletal muscle mitochondria from R163C-RyR1 mice have accumulated more calcium within their matrix (presumably mainly as Ca^{2+} -phosphate precipitate (110)) than controls under basal conditions (i.e. in the absence of a fulminant MH episode). One possible caveat is that EGTA used in the isolation buffer could have reduced the free Ca^{2+} within mitochondria thereby resulting in an underestimate of mitochondrial calcium. Despite this possible limitation, we were able to identify significant differences in total matrix calcium between genotypes. Considering that a subpopulation of mitochondria has been found closely attached to SR (87,88), and these mitochondria are exposed to higher local resting Ca^{2+} concentration in skeletal muscle (89,90), it is likely that our calcium values represent an underestimation of those actually found in mitochondria closely associated with SR (90). Possible consequences of higher mitochondrial calcium might be mitochondrial swelling, as it has been observed in skeletal muscle from aged Y522S MHS mice (44), and mitochondria loss, known to occur in CCD skeletal muscle fibers (2).

However, chronically elevated resting Ca^{2+} in R163C skeletal elicited not only the maintenance of a fast-twitch fiber program with clear mitochondrial defects in terms of number and function (permeabilized muscle, and intact muscle) but also the development of an insulin resistance-like phenotype as part of a metabolic adaptation to the R163C RyR1 mutation.

Several possibilities may explain the differences in State 3-dependent oxygen uptake between WT and R163C mice. First, the mitochondrial pellet may be contaminated with non-mitochondrial protein (i.e. myosin, fragmented myofibrils or myoglobin). Any contaminating protein is assayed in the BCA reaction (56), resulting in an underestimation of the oxygen consumption rate when related to mitochondrial protein concentration. The normalization of oxygen uptake rates to a mitochondrial enzyme such as cytochrome *c* oxidase rather than to mitochondrial protein may eliminate this problem in normal studies, but is not appropriate in diseased muscle where specific mitochondrial enzymes may be selectively depressed. The presence of a significant contamination of non-mitochondrial protein was excluded in our study based on the low recovery of

both a highly abundant protein such as myoglobin (0.03% and 0.08% in WT and R163C; **Figure 1C**) and the oligomycin-resistant ATPase activity (111,112) (1.6% and 2.0% in WT and R163C) in the mitochondrial fractions. These results supported the notion that the contamination from cytosolic (myoglobin) or sarcoplasmic reticulum/plasmalemma (oligomycin-resistant ATPase) was negligible (<1% in average).

A second possibility is that slow respiratory rates with all substrates with loose coupling –as in the case with R163C (**Tables I** and **II**)– may indicate a damaged preparation. However, the biochemical characteristics of muscle mitochondria from WT -run in parallel to those of R163C- were of similar or higher quality than those published by others (**Table I**) suggesting that this is not the case.

Another possible explanation is that during mitochondria isolation, homogenization of diseased muscle may free a higher percentage of total muscle mitochondrial fractions with a higher proportion of damaged organelles, resulting in a falsely low respiration rate. If this hypothesis is correct, oxygen uptake rates should be lowest in preparations with higher mitochondrial protein yields. This alternative can also be excluded because the mitochondrial protein yield from R163C and WT mice were not significantly different (**Table I**) whereas the State 3-dependent oxygen uptake in R163C was $62 \pm 3\%$ of WT (**Table II**). In addition, data on the maximal oxygen uptake sustained by NADH obtained with permeabilized muscle to test for mitochondrial function *in situ* was $52 \pm 9\%$ that of WT, similar to the differences seen with isolated mitochondria supplemented with an NAD-linked substrate (**Table II**). The slight discrepancy between these numbers could be explained by considering that all mitochondrial populations are assayed in permeabilized muscle with limited cytoskeletal disruption, whereas the preparation with isolated mitochondria is likely to be more enriched with intact, less dysfunctional organelles (113), suggesting that the changes observed with isolated mitochondria could underestimate the putative mitochondrial dysfunction *in vivo*.

In this study no attempt was made to differentially isolate subsarcolemmal (SSM) and intermyofibrillar (IMF) mitochondrial populations, mitochondria with different morphology, organ localization and biochemical characteristics (114,115); however, it is likely that our preparation was richer in SSM than IMF due to the lack of protease use during the isolation procedure (which

helps to improve the recovery of IMF) and based on the rates of State 3 oxygen consumption rates (116,117). The electron transport chain activity of SSM has been found decreased in individuals with T2D (118,119) to values similar to ours (2 to 3-fold lower State 3 oxygen uptake using NAD- and FAD-linked substrates). Considering that SSM provide energy for membrane-related processes, including processes involved in insulin action, glucose uptake and storage (115,118), then the presence of dysfunctional SSM in R163C could be result in an insulin resistance-like phenotype.

Taken together, these data support the hypothesis that the R163C RyR1 mutation in skeletal muscle results in defects in mitochondrial number and function. Moreover, the mutation also elicited lower glucose utilization by both OXPHOS and glycolysis (**Table III**). To gain insight into the interaction between pathways, we used the DAVID Gene Functional Classification Tool (67,68) to condense the list of pathways enriched in the proteins and/or transcripts found altered in R163C mice. The resulting distribution highlighted overrepresented Gene Ontology (GO) categories. Besides the OXPHOS pathway, others that ranked high in the hierarchy were the following ones: Cn/NFAT, insulin, and calcium and muscle contraction (**Figure 5**).

The specific regulation of slow fiber-specific genes is controlled by the calcineurin (Cn) pathway (95). Cn, a Ca^{2+} -activated, calmodulin-dependent protein Ser/Thr phosphatase that senses intracellular Ca^{2+} levels, dephosphorylates NFAT, which translocates to the nucleus and regulates the transcription of target genes (95). Transgenic mice over-expressing an activated form of Cn in skeletal muscle presented a marked shift in glucose (decreased glucose oxidation with increased glycogen formation) and lipid (increased fatty acid oxidation and mitochondria biogenesis) metabolism *via* coordinated expression of metabolic genes, as well as transcription regulators, including PPAR δ , PPAR α , and PGC1- α (96), with increased expression of slow contractile machinery (97). Conversely, pharmacological inhibition of Cn activity induces a slow to fast myosin ATPase transformation in rat soleus muscle (95). The expression of downstream Cn/NFAT-regulated genes provides a reliable measure of Cn activation. To test the hypothesis that the Cn-mediated pathway was inactive in R163C mice, we evaluated the protein expression of Cn, RCAN (endogenous inhibitors of Cn; (120,121)), PGC1- α and

myoglobin (96,97), glycogen and triglyceride contents (96), and the transcript expression of myosin heavy chains isoforms (*Myh 1* (type IIX/D), *Myh2* (type IIA), *Myh4* (type IIB) *Myh 7* (type I); (97)). As predicted, in R163C skeletal muscle, we observed over-expression of RCAN3 and lower expression of Cn (**Figure 5**). This outcome was somewhat similar to that encountered by cells incubated with thapsigargin, an inhibitor of SR Ca^{2+} -ATPase, in which the short-term elevation in Ca^{2+} resulted in an increased expression of the Cn inhibitor RCAN1 (122). It has been shown that over-expression of RCAN3 in Jurkat cells inhibits calcium-Cn mediated NFAT nuclear translocation and RCAN1 gene expression. Furthermore, RCAN3 gene expression is neither under intracellular calcium regulation nor under the physiological regulation of Cn activity (121). It has been suggested that RCAN3 may interact with one of the catalytic isoforms of Cn different from that that interacts with RCAN1, indicating different roles for RCAN-Cn (123). Consistent with this concept, not all Cn activity seemed to be halted, for some NFAT isoforms (likely c2, c3, and c4; (124) but not others (e.g., NFATc1) are expected to activate the fiber type IID/X expression and repress type I expression. Under *in vivo* conditions, the rapid activation of calcium uptake sites and calcium exchangers evoked by RyR-mediated local calcium signals allow mitochondria to respond rapidly to single calcium spikes (90). The higher cytosolic calcium, in addition to the proximity to RyR1, allows mitochondria to buffer the excess of calcium at the expense of the dissipation of the electrochemical gradient (uncoupling), preventing the incorporation of nDNA-encoded proteins. Among them, probably those required for the translation of mitochondrial proteins (e.g., aminoacyl tRNA synthetases), resulting in a mitochondrial protein synthesis that lags behind the nuclear one. This would explain the increased mitochondrial calcium content and the relative lower protein expression of mtDNA-encoded subunits. The development of mitochondrial dysfunction could be understood as the result of calcium recycling (*in vivo*) in addition to a lower OXPHOS capacity in Complexes with mtDNA-encoded subunits (*in vivo* and *in vitro*). Central to this mitochondrial dysfunction is the increase in ROS (2-3 fold). Increases in oxidative stress lead to the phosphorylation of ERK1/2 (activation), which sustains the fast-twitch fiber type program, reinforcing the NFAT-Cn pathway. The lower

activation of AMPK observed in this study indicates that the production of ATP (via glycolysis and oxidative phosphorylation) matches the energy expenditure of R163C muscle at rest. Furthermore, if AMP is the main activator of AMPK, then a lower steady-state concentration of AMP in R163C muscle could be achieved by decreasing the activity of adenylate kinase (125), and/or by increasing the AMP deaminase activity (which is calcium-activated (126,127)). Other contributing factors could involve a negative feedback on any of the upstream kinases of AMPK by hormone or metabolite-mediated cascade signaling (128). In any case, the lower AMPK activation in R163C muscle resulted in lower phosphorylation of ACC2, increased activity of ACC2, and lower fatty-acid oxidation. The lower activation of AMPK leads to inactivation of PPAR α , preventing the transcription of genes in the fatty-acid oxidation pathway and increasing triglyceride content in muscle (129). Inactivation of AMPK leads to a decreased transcription of myocyte enhancer factor 2C (MEF2C) and dephosphorylation of PGC1- α , which in turn decreases mitochondrial content, oxidative capacity, transcription/activity of the antioxidant enzyme MnSOD, and oxidative-fiber type composition. Lower AMPK activity leads to lower translocation of GLUT4 (decreased glucose uptake) and lower glycogen deposits (**Figure 5**).

The functional consequence of deficient fatty-acid oxidation and impaired ETC activity might be the accumulation of fat and fat metabolites (diacylglycerol, ceramide, fatty acylCoA) that can activate Ser kinases that inhibit insulin signaling and glucose transport (130-133), resulting in a decrease in insulin sensitivity. Alternatively, activated ERK1/2 phosphorylates S612-IRS-1 and inhibits its association with PI3-K and in turn Akt activation, thus generating a negative feedback loop that down-regulates insulin stimulated glucose uptake (134). In any case, the increased MAP kinase/ERK signaling along with the decrease in mitochondrial proteins observed in muscle from obese individuals or with Type 2 diabetes (135-137) underlines the

biochemical similarities between MH muscle and insulin-resistant muscle. The presence of dysfunctional mitochondria, lipid deposits, lower glycogen, lower glucose uptake and/or utilization, and increased ROS in R163C skeletal muscle (this study), higher blood insulin levels (absolute values or normalized to glucose) in malignant hyperthermia susceptible individuals (5,138), higher baseline [lactate] and [lactate]/[pyruvate] ratio in MHS pigs than MH-non susceptible (139) resembles the characteristics presented by individuals with insulin resistance and Type 2 diabetes. However, opposite to these cases (136,140), no decrease in the expression of genes encoding proteins of mitochondrial OXPHOS in R163C skeletal muscle were observed, pointing at the metabolic adaptive response that allows R163C mutant carriers to develop a normal life. If exposed to triggers such as halogenated anesthetics or higher ambient temperatures, the dysfunctional mitochondria, in addition to the lower glucose uptake in skeletal muscle of individuals carrying this RyR1 mutation, would attempt to dampen the deleterious effects (uncoupling, heat production by mitochondria, lactic acid production) initiated by MH triggers

Then, the key question would be: what is the link between chronically elevated Ca²⁺ in muscle and the appearance of a phenotype with characteristics similar to those of insulin resistance? It has been reported that insulin elicits either localized (near membrane; (141)) or global (142) Ca²⁺ increases, and that such increases are sufficient to activate a CaMKII-dependent signaling pathway in rat soleus (143). Thus, an adaptive response to cope with a “leaky” RyR1 would be to increase insulin resistance in muscle to attenuate/counteract the insulin response that could be already potentiated by the relatively higher resting intracellular calcium. This could explain the occurrence of MH-like episodes in acute metabolic complications of diabetes such as diabetic ketoacidosis and hyperglycemic hyperosmolar nonketotic syndrome (144-146).

REFERENCES

1. Denborough, M. A., Forster, J. F., Lovell, R. R., Maplestone, P. A., and Villiers, J. D. (1962) *Br J Anaesth* **34**, 395-396
2. Dubowitz, V., and Pearce, A. G. (1960) *Lancet* **2**, 23-24
3. Magee, K. R., and Shy, G. M. (1956) *Brain* **79**, 610-621
4. Robinson, R., Carpenter, D., Shaw, M. A., Halsall, J., and Hopkins, P. (2006) *Hum Mutat* **27**, 977-989

5. Denborough, M. A., Forster, J. F., Hudson, M. C., Carter, N. G., and Zapf, P. (1970) *Lancet* **1**, 1137-1138
6. Robinson, R. L., Brooks, C., Brown, S. L., Ellis, F. R., Halsall, P. J., Quinnell, R. J., Shaw, M. A., and Hopkins, P. M. (2002) *Hum Mutat* **20**, 88-97
7. Rueffert, H., Olthoff, D., Deutrich, C., Schober, R., and Froster, U. G. (2004) *Am J Med Genet A* **124A**, 248-254
8. Shuaib, A., Paasuke, R. T., and Brownell, K. W. (1987) *Medicine (Baltimore)* **66**, 389-396
9. Loke, J., and MacLennan, D. H. (1998) *Am J Med* **104**, 470-486
10. Aleman, M., Riehl, J., Aldridge, B. M., Lecouteur, R. A., Stott, J. L., and Pessah, I. N. (2004) *Muscle Nerve* **30**, 356-365
11. Wappler, F. (2001) *Eur J Anaesthesiol* **18**, 632-652
12. Gillard, E. F., Otsu, K., Fujii, J., Khanna, V. K., de Leon, S., Derdemezi, J., Britt, B. A., Duff, C. L., Worton, R. G., and MacLennan, D. H. (1991) *Genomics* **11**, 751-755
13. Quane, K. A., Healy, J. M. S., Keating, K. E., Manning, B. M., Couch, F. J., Palmucci, L. M., Doriguzzi, C., Fagerlund, T. H., Berg, K., Ording, H., Bendixen, D., Mortier, W., Linz, U., Muller, C. R., and McCarthy, T. V. (1993) *Nat Genet* **5**, 51-55
14. Zhang, Y., Chen, H. S., Khanna, V. K., De Leon, S., Phillips, M. S., Schappert, K., Britt, B. A., Browell, A. K., and MacLennan, D. H. (1993) *Nat Genet* **5**, 46-50
15. Davis, M. R., Haan, E., Jungbluth, H., Sewry, C., North, K., Muntoni, F., Kuntzer, T., Lamont, P., Bankier, A., Tomlinson, P., Sanchez, A., Walsh, P., Nagarajan, L., Oley, C., Colley, A., Gedeon, A., Quinlivan, R., Dixon, J., James, D., Muller, C. R., and Laing, N. G. (2003) *Neuromuscul Disord* **13**, 151-157
16. Jungbluth, H., Beggs, A., Bonnemann, C., Bushby, K., Ceuterick-de Groote, C., Estournet-Mathiaud, B., Goemans, N., Guicheney, P., Lescure, A., Lunardi, J., Muntoni, F., Quinlivan, R., Sewry, C., Straub, V., Treves, S., and Ferreiro, A. (2004) *Neuromuscul Disord* **14**, 754-766
17. Jungbluth, H., Zhou, H., Hartley, L., Halliger-Keller, B., Messina, S., Longman, C., Brockington, M., Robb, S. A., Straub, V., Voit, T., Swash, M., Ferreiro, A., Bydder, G., Sewry, C. A., Muller, C., and Muntoni, F. (2005) *Neurology* **65**, 1930-1935
18. Jurkat-Rott, K., McCarthy, T., and Lehmann-Horn, F. (2000) *Muscle Nerve* **23**, 4-17
19. McCarthy, T. V., Quane, K. A., and Lynch, P. J. (2000) *Hum Mutat* **15**, 410-417
20. Monnier, N., Romero, N. B., Lerale, J., Landrieu, P., Nivoche, Y., Fardeau, M., and Lunardi, J. (2001) *Hum Mol Genet* **10**, 2581-2592
21. Tilgen, N., Zorzato, F., Halliger-Keller, B., Muntoni, F., Sewry, C., Palmucci, L. M., Schneider, C., Hauser, E., Lehmann-Horn, F., Muller, C. R., and Treves, S. (2001) *Hum Mol Genet* **10**, 2879-2887
22. Treves, S., Anderson, A. A., Ducreux, S., Divet, A., Bleunven, C., Grasso, C., Paesante, S., and Zorzato, F. (2005) *Neuromuscul Disord* **15**, 577-587
23. Monnier, N., Ferreiro, A., Marty, I., Labarre-Vila, A., Mezin, P., and Lunardi, J. (2003) *Hum Mol Genet* **12**, 1171-1178
24. Sambuughin, N., McWilliams, S., de Bantel, A., Sivakumar, K., and Nelson, T. E. (2001) *Am J Hum Genet* **69**, 204-208
25. Treves, S., Jungbluth, H., Muntoni, F., and Zorzato, F. (2008) *Curr Opin Pharmacol* **8**, 319-326
26. Carpenter, D., Ringrose, C., Leo, V., Morris, A., Robinson, R. L., Halsall, P. J., Hopkins, P. M., and Shaw, M. A. (2009) *BMC Med Genet* **10**, 104
27. Wu, S., Ibarra, M. C., Malicdan, M. C., Murayama, K., Ichihara, Y., Kikuchi, H., Nonaka, I., Noguchi, S., Hayashi, Y. K., and Nishino, I. (2006) *Brain* **129**, 1470-1480
28. Yang, T., Ta, T. A., Pessah, I. N., and Allen, P. D. (2003) *J Biol Chem* **278**, 25722-25730
29. Yang, T., Riehl, J., Esteve, E., Matthaei, K. I., Goth, S., Allen, P. D., Pessah, I. N., and Lopez, J. R. (2006) *Anesthesiology* **105**, 1164-1175
30. Yang, T., Esteve, E., Pessah, I. N., Molinski, T. F., Allen, P. D., and Lopez, J. R. (2007) *Am J Physiol Cell Physiol* **292**, C1591-1598
31. Cherednichenko, G., Hurne, A. M., Fessenden, J. D., Lee, E. H., Allen, P. D., Beam, K. G., and Pessah, I. N. (2004) *Proc Natl Acad Sci U S A* **101**, 15793-15798

32. Cherednichenko, G., Ward, C. W., Feng, W., Cabrales, E., Michaelson, L., Samsó, M., Lopez, J. R., Allen, P. D., and Pessah, I. N. (2008) *Mol Pharmacol* **73**, 1203-1212
33. Wilson, R. D. M., Traber, D. L. P., Allen, C. R. M. D. P., and Priano, L. L. P. (1971) *Southern Medical Journal* **64**, 411-414
34. Wang, J. K., Moffitt, E. A., and Rosevear, J. W. (1969) *Anesthesiology* **30**, 439-442
35. Britt, B. A., Kalow, W., Gordon, A., Humphrey, J. G., and Rewcastle, N. B. (1973) *Can Anaesth Soc J* **20**, 431-467
36. Britt, B. A., Kalow, W., and Endrenyi, L. (1973) In: Gordon, RA, Britt, BA, and Kalow, W (eds.). *International Symposium on Malignant Hyperthermia. Charles C. Thomas, Springfield, Ill*, 387
37. Ellis, F. R., Keane, N. P., and Harriman, D. G. (1973) *Proc R Soc Med* **66**, 66-67
38. Fenoglio, J. J., Jr., and Irely, N. S. (1977) *Am J Pathol* **89**, 51-58
39. Schiller, H. H., and Mair, W. G. P. (1974) *Journal of the Neurological Sciences* **21**, 93-100
40. Mezin, P., Payen, J. F., Bosson, J. L., Brambilla, E., and Stieglitz, P. (1997) *Br J Anaesth* **79**, 327-331
41. Foster, P. S., Hopkinson, K., and Denborough, M. A. (1989) *Muscle Nerve* **12**, 390-396
42. Payen, J. F., Bosson, J. L., Bourdon, L., Jacquot, C., Le Bas, J. F., Stieglitz, P., and Benabid, A. L. (1993) *Anesthesiology* **78**, 848-855
43. Payen, J. F., Bourdon, L., Mezin, P., Jacquot, C., le Bas, J. F., Stieglitz, P., and Benabid, A. L. (1991) *Lancet* **337**, 1550-1551
44. Durham, W. J., Aracena-Parks, P., Long, C., Rossi, A. E., Goonasekera, S. A., Boncompagni, S., Galvan, D. L., Gilman, C. P., Baker, M. R., Shirokova, N., Protasi, F., Dirksen, R., and Hamilton, S. L. (2008) *Cell* **133**, 53-65
45. Yang, T., Riehl, J., Esteve, E., Matthaei, K. I., Goth, S., Allen, P. D., Pessah, I. N., and Lopez, J. R. (2006) *Anesthesiology* **105**, 1164-1175
46. Bonefeld, B. E., Elfving, B., and Wegener, G. (2008) *Synapse* **62**, 302-309
47. Gubern, C., Hurtado, O., Rodriguez, R., Morales, J. R., Romera, V. G., Moro, M. A., Lizasoain, I., Serena, J., and Mallolas, J. (2009) *BMC Mol Biol* **10**, 57
48. Pfaffl, M. W., Tichopad, A., Prgomet, C., and Neuvians, T. P. (2004) *Biotechnol Lett* **26**, 509-515
49. Pattyn, F., Speleman, F., De Paepe, A., and Vandesompele, J. (2003) *Nucleic Acids Res* **31**, 122-123
50. Andersen, C. L., Jensen, J. L., and Orntoft, T. F. (2004) *Cancer Res* **64**, 5245-5250
51. Elfering, S. L., Haynes, V. L., Traaseth, N. J., Ettl, A., and Giulivi, C. (2004) *Am J Physiol Heart Circ Physiol* **286**, H22-29
52. Mickelson, J. R., Greaser, M. L., and Marsh, B. B. (1980) *Anal Biochem* **109**, 255-260
53. Schwerzmann, K., Cruz-Orive, L. M., Eggman, R., Sanger, A., and Weibel, E. R. (1986) *J Cell Biol* **102**, 97-103
54. Gazzotti, P., Flura, M., and Gloor, M. (1985) *Biochem Biophys Res Commun* **127**, 358-365
55. Bolender, R. P., Paumgartner, D., Losa, G., Muellener, D., and Weibel, E. R. (1978) *J Cell Biol* **77**, 565-583
56. Wiechelman, K. J., Braun, R. D., and Fitzpatrick, J. D. (1988) *Anal Biochem* **175**, 231-237
57. Kuznetsov, A. V., Veksler, V., Gellerich, F. N., Saks, V., Margreiter, R., and Kunz, W. S. (2008) *Nat Protoc* **3**, 965-976
58. Smith, M. J., and Jeffrey, S. W. (1956) *Biochem J* **63**, 524-528
59. Barrientos, A. (2002) *Methods* **26**, 307-316
60. Hatefi, Y., and Stiggall, D. L. (1978) *Methods in Enzymology* **53**, 21-27
61. Fujisawa, Y., Kato, K., and Giulivi, C. (2009) *Biochem J* **423**, 219-231
62. Missihoun, C., Zisa, D., Shabbir, A., Lin, H., and Lee, T. (2009) *Mol Cell Biochem* **321**, 45-52
63. Sarkela, T. M., Berthiaume, J., Elfering, S., Gybina, A. A., and Giulivi, C. (2001) *J Biol Chem* **276**, 6945-6949
64. Ashcroft, S. J. H., and Pereira, C. (2002) *Biochemical Society Transactions* **30**, A114
65. Lo, S., Russell, J. C., and Taylor, A. W. (1970) *J Appl Physiol* **28**, 234-236
66. Lebaron, F. N., and Folch, J. (1959) *J Neurochem* **4**, 1-8
67. Dennis, G., Jr., Sherman, B. T., Hosack, D. A., Yang, J., Gao, W., Lane, H. C., and Lempicki, R. A. (2003) *Genome Biol* **4**, P3
68. Huang da, W., Sherman, B. T., and Lempicki, R. A. (2009) *Nat Protoc* **4**, 44-57

69. Buck, E. D., Nguyen, H. T., Pessah, I. N., and Allen, P. D. (1997) *J Biol Chem* **272**, 7360-7367
70. Chance, B. (1959) Quantitative aspects of the control of oxygen utilization. in *A Ciba Foundation Symposium on the Regulation of Cell Metabolism* (Wolstenholme, O. C. ed.), J. & A. Churchill Ltd., London. pp 91-121
71. Estabrook, R. W. (1967) *Methods in Enzymology* **10**, 41-47
72. Chance, B., and Williams, G. R. (1955) *Nature* **175**, 1120-1121
73. Boushel, R., Gnaiger, E., Schjerling, P., Skovbro, M., Kraunsoe, R., and Dela, F. (2007) *Diabetologia* **50**, 790-796
74. Gellerich, F. N., Deschauer, M., Chen, Y., Muller, T., Neudecker, S., and Zierz, S. (2002) *Biochim Biophys Acta* **1556**, 41-52
75. Rustin, P., Chretien, D., Bourgeron, T., Gerard, B., Rotig, A., Saudubray, J. M., and Munnich, A. (1994) *Clin Chim Acta* **228**, 35-51
76. Lopez, J. R., Linares, N., Pessah, I. N., and Allen, P. D. (2005) *Am J Physiol Cell Physiol* **288**, C606-612
77. O'Brien, P. J., Klip, A., Britt, B. A., and Kalow, B. I. (1990) *Can J Vet Res* **54**, 83-92
78. O'Brien, P. J., Pook, H. A., Klip, A., Britt, B. A., Kalow, B. I., McLaughlin, R. N., Scott, E., and Elliott, M. E. (1990) *Res Vet Sci* **48**, 124-128
79. Mezon, B. J., Wrogemann, K., and Blanchaer, M. C. (1974) *Can J Biochem* **52**, 1024-1032
80. Wrogemann, K., Jacobson, B. E., and Blanchaer, M. C. (1973) *Arch Biochem Biophys* **159**, 267-278
81. Ichas, F., and Mazat, J. P. (1998) *Biochim Biophys Acta* **1366**, 33-50
82. LeBlondel, G., Ducouret, C., and Allain, P. (1988) *Biol Trace Elem Res* **16**, 115-127
83. Everts, M. E., Lomo, T., and Clausen, T. (1993) *Acta Physiol Scand* **147**, 357-368
84. Zimmermann, P., Weiss, U., Classen, H. G., Wendt, B., Epple, A., Zollner, H., Temmel, W., Weger, M., and Porta, S. (2000) *Life Sci* **67**, 949-958
85. Leblondel, G., Mauras, Y., Cailleux, A., and Allain, P. (2001) *Biol Trace Elem Res* **83**, 191-206
86. Yoshida, M., Yonetani, A., Shirasaki, T., and Wada, K. (2006) *Am J Physiol Regul Integr Comp Physiol* **290**, R449-455
87. Rizzuto, R., Brini, M., Murgia, M., and Pozzan, T. (1993) *Science* **262**, 744-747
88. Rizzuto, R., Pinton, P., Carrington, W., Fay, F. S., Fogarty, K. E., Lifshitz, L. M., Tuft, R. A., and Pozzan, T. (1998) *Science* **280**, 1763-1766
89. Feng, L., Pereira, B., and Kraus-Friedmann, N. (1992) *Cell Calcium* **13**, 79-87
90. Szalai, G., Csordas, G., Hantash, B. M., Thomas, A. P., and Hajnoczky, G. (2000) *J Biol Chem* **275**, 15305-15313
91. Taylor, W. M., Prpic, V., Exton, J. H., and Bygrave, F. L. (1980) *Biochem J* **188**, 443-450
92. Williams, R. S. (1986) *J Biol Chem* **261**, 12390-12394
93. Williams, R. S., Garcia-Moll, M., Mellor, J., Salmons, S., and Harlan, W. (1987) *J Biol Chem* **262**, 2764-2767
94. Ross-Inta, C., Tsai, C.-Y., and Giulivi, C. (2008) *Biosci. Rep.* **28**, 239-249
95. Chin, E. R., Olson, E. N., Richardson, J. A., Yang, Q., Humphries, C., Shelton, J. M., Wu, H., Zhu, W., Bassel-Duby, R., and Williams, R. S. (1998) *Genes Dev.* **12**, 2499-2509
96. Long, Y. C., Glund, S., Garcia-Roves, P. M., and Zierath, J. R. (2007) *J. Biol. Chem.* **282**, 1607-1614
97. Naya, F. J., Mercer, B., Shelton, J., Richardson, J. A., Williams, R. S., and Olson, E. N. (2000) *J. Biol. Chem.* **275**, 4545-4548
98. Mu, X., Brown, L. D., Liu, Y., and Schneider, M. F. (2007) *Physiol. Genomics* **30**, 300-312
99. Hawley, S. A., Pan, D. A., Mustard, K. J., Ross, L., Bain, J., Edelman, A. M., Frenguelli, B. G., and Hardie, D. G. (2005) *Cell Metab* **2**, 9-19
100. Cross, H. R., Murphy, E., Bolli, R., Ping, P., and Steenbergen, C. (2002) *J Mol Cell Cardiol* **34**, 361-367
101. Edmondson, R. D., Vondriska, T. M., Biederman, K. J., Zhang, J., Jones, R. C., Zheng, Y., Allen, D. L., Xiu, J. X., Cardwell, E. M., Pisano, M. R., and Ping, P. (2002) *Mol Cell Proteomics* **1**, 421-433
102. Giulivi, C., and Ousler, M. J. (2003) *Signal Transduction by Reactive Oxygen and Nitrogen Species: Pathways and Chemical Principles.* (M Torres, J Fukuto, and HJ Forman, eds.), 311-332
103. Crossthwaite, A. J., Hasan, S., and Williams, R. J. (2002) *J Neurochem* **80**, 24-35
104. Guyton, K. Z., Liu, Y., Gorospe, M., Xu, Q., and Holbrook, N. J. (1996) *J Biol Chem* **271**, 4138-4142

105. Hannken, T., Schroeder, R., Zahner, G., Stahl, R. A., and Wolf, G. (2000) *J Am Soc Nephrol* **11**, 1387-1397
106. Lin, H. Y., Michtalik, H. J., Zhang, S., Andersen, T. T., Van Riper, D. A., Davies, K. K., Ermak, G., Petti, L. M., Nachod, S., Narayan, A. V., Bhatt, N., and Crawford, D. R. (2003) *Free Radic Biol Med* **35**, 528-539
107. Shi, H., Zeng, C., Ricome, A., Hannon, K. M., Grant, A. L., and Gerrard, D. E. (2007) *Am J Physiol Cell Physiol* **292**, C1681-1689
108. Shi, H., Scheffler, J. M., Pleitner, J. M., Zeng, C., Park, S., Hannon, K. M., Grant, A. L., and Gerrard, D. E. (2008) *FASEB J.* **22**, 2990-3000
109. Marban, E., Rink, T. J., Tsien, R. W., and Tsien, R. Y. (1980) *Nature* **286**, 845-850
110. Argaud, L., Gateau-Roesch, O., Augeul, L., Couture-Lepetit, E., Loufouat, J., Gomez, L., Robert, D., and Ovize, M. (2008) *Am J Physiol Heart Circ Physiol* **294**, H386-391
111. Fernandez, J. L., Roseblatt, M., and Hidalgo, C. (1980) *Biochim Biophys Acta* **599**, 552-568
112. Harigaya, S., Ogawa, Y., and Sugita, H. (1968) *J Biochem* **63**, 324-331
113. Andrienko, T., Kuznetsov, A. V., Kaambre, T., Usson, Y., Orosco, A., Appaix, F., Tiivel, T., Sikk, P., Vendelin, M., Margreiter, R., and Saks, V. A. (2003) *J Exp Biol* **206**, 2059-2072
114. Palmer, J. W., Tandler, B., and Hoppel, C. L. (1977) *J Biol Chem* **252**, 8731-8739
115. Riva, A., Tandler, B., Loffredo, F., Vazquez, E., and Hoppel, C. (2005) *Am J Physiol Heart Circ Physiol* **289**, H868-872
116. Manneschi, L., and Federico, A. (1995) *J Neurol Sci* **128**, 151-156
117. Bizeau, M. E., Willis, W. T., and Hazel, J. R. (1998) *J Appl Physiol* **85**, 1279-1284
118. Ritov, V. B., Menshikova, E. V., Azuma, K., Wood, R., Toledo, F. G. S., Goodpaster, B. H., Ruderman, N. B., and Kelley, D. E. (2010) *Am. J. Physiol.* **298**, E49-E58
119. Benton, C. R., Nickerson, J. G., Lally, J., Han, X.-X., Holloway, G. P., Glatz, J. F. C., Luiken, J. J. F. P., Graham, T. E., Heikkila, J. J., and Bonen, A. (2008) *J. Biol. Chem.* **283**, 4228-4240
120. Lin, H. Y., Michtalik, H. J., Zhang, S., Andersen, T. T., Van Riper, D. A., Davies, K. K. J. A., Ermak, G., Petti, L. M., Nachod, S., Narayan, A. V., Bhatt, N., and Crawford, D. R. (2003) *Free Radical Biology and Medicine* **35**, 528-539
121. Mulero, M. C., Aubareda, A., Schluter, A., and Perez-Riba, M. (2007) *Biochim Biophys Acta* **1773**, 330-341
122. Zhao, P., Xiao, X., Kim, A. S., Leite, M. F., Xu, J., Zhu, X., Ren, J., and Li, J. (2008) *Experimental Biology and Medicine* **233**, 1289-1300
123. Porta, S., Marti, E., de la Luna, S., and Arbones, M. L. (2007) *Eur J Neurosci* **26**, 1213-1226
124. Calabria, E., Ciciliot, S., Moretti, I., Garcia, M., Picard, A., Dyar, K. A., Pallafacchina, G., Tothova, J., Schiaffino, S., and Murgia, M. (2009) *Proc Natl Acad Sci U S A* **106**, 13335-13340
125. Hancock, C. R., Brault, J. J., Wiseman, R. W., Terjung, R. L., and Meyer, R. A. (2005) *Am J Physiol Cell Physiol* **288**, C1298-1304
126. Engstrom, I., Waldenstrom, A., and Ronquist, G. (1996) *Scand J Clin Lab Invest* **56**, 345-350
127. Almaraz, L., and Garcia-Sancho, J. (1989) *FEBS Lett* **244**, 417-420
128. Imai, K., Inukai, K., Ikegami, Y., Awata, T., and Katayama, S. (2006) *Biochem Biophys Res Commun* **351**, 595-601
129. Yamauchi, T., Kamon, J., Minokoshi, Y., Ito, Y., Waki, H., Uchida, S., Yamashita, S., Noda, M., Kita, S., Ueki, K., Eto, K., Akanuma, Y., Froguel, P., Foufelle, F., Ferre, P., Carling, D., Kimura, S., Nagai, R., Kahn, B. B., and Kadowaki, T. (2002) *Nat Med* **8**, 1288-1295
130. Chavez, J. A., Knotts, T. A., Wang, L. P., Li, G., Dobrowsky, R. T., Florant, G. L., and Summers, S. A. (2003) *J Biol Chem* **278**, 10297-10303
131. Chavez, J. A., and Summers, S. A. (2003) *Arch Biochem Biophys* **419**, 101-109
132. Adams, J. M., 2nd, Pratipanawatr, T., Berria, R., Wang, E., DeFronzo, R. A., Sullards, M. C., and Mandarino, L. J. (2004) *Diabetes* **53**, 25-31
133. Yu, C., Chen, Y., Cline, G. W., Zhang, D., Zong, H., Wang, Y., Bergeron, R., Kim, J. K., Cushman, S. W., Cooney, G. J., Atcheson, B., White, M. F., Kraegen, E. W., and Shulman, G. I. (2002) *J Biol Chem* **277**, 50230-50236
134. Huang, C., Thirone, A. C., Huang, X., and Klip, A. (2005) *J Biol Chem* **280**, 19426-19435

135. Hwang, H., Bowen, B. P., Lefort, N., Flynn, C. R., De Filippis, E. A., Roberts, C., Smoke, C. C., Meyer, C., Hvalby, K., Yi, Z., and Mandarino, L. J. (2010) *Diabetes* **59**, 33-42
136. Patti, M. E., Butte, A. J., Crunkhorn, S., Cusi, K., Berria, R., Kashyap, S., Miyazaki, Y., Kohane, I., Costello, M., Saccone, R., Landaker, E. J., Goldfine, A. B., Mun, E., DeFronzo, R., Finlayson, J., Kahn, C. R., and Mandarino, L. J. (2003) *Proc Natl Acad Sci U S A* **100**, 8466-8471
137. Krook, A., Bjornholm, M., Galuska, D., Jiang, X. J., Fahlman, R., Myers, M. G., Jr., Wallberg-Henriksson, H., and Zierath, J. R. (2000) *Diabetes* **49**, 284-292
138. Campbell, I. T., Ellis, F. R., and Evans, R. T. (1981) *Anesthesiology* **55**, 46-52
139. Bina, S., Cowan, G., Karaian, J., Muldoon, S., Mongan, P., and Bunger, R. (2006) *Anesthesiology* **104**, 90-100
140. Mootha, V. K., Lindgren, C. M., Eriksson, K. F., Subramanian, A., Sihag, S., Lehar, J., Puigserver, P., Carlsson, E., Ridderstrale, M., Laurila, E., Houstis, N., Daly, M. J., Patterson, N., Mesirov, J. P., Golub, T. R., Tamayo, P., Spiegelman, B., Lander, E. S., Hirschhorn, J. N., Altshuler, D., and Groop, L. C. (2003) *Nat Genet* **34**, 267-273
141. Bruton, J. D., Katz, A., and Westerblad, H. (1999) *Proc Natl Acad Sci U S A* **96**, 3281-3286
142. Espinosa, A., Estrada, M., and Jaimovich, E. (2004) *J Endocrinol* **182**, 339-352
143. Wright, D. C., Fick, C. A., Olesen, J. B., Lim, K., Barnes, B. R., and Craig, B. W. (2004) *Life Sci* **74**, 815-825
144. Venkatraman, R., and Singhi, S. C. (2006) *Indian J Pediatr* **73**, 55-60
145. Hollander, A. S., Olney, R. C., Blackett, P. R., and Marshall, B. A. (2003) *Pediatrics* **111**, 1447-1452
146. Kilbane, B. J., Mehta, S., Backeljauw, P. F., Shanley, T. P., and Crimmins, N. A. (2006) *Pediatric Critical Care Medicine* **7**, 169-173
147. Bocek, R. M., Basinger, G. M., and Beatty, C. H. (1966) *Am J Physiol* **210**, 1108-1111
148. Bocek, R. M., and Beatty, C. H. (1966) *J Histochem Cytochem* **14**, 549-559
149. Bocek, R. M., Peterson, R. D., and Beatty, C. H. (1966) *Am J Physiol* **210**, 1101-1107
150. Nishiyama, A. (1966) *Acta Med Okayama* **20**, 137-146
151. Delp, M. D., and Duan, C. (1996) *J Appl Physiol* **80**, 261-270
152. Bookelman, H., Trijbels, J. M., Sengers, R. C., Janssen, A. J., Veerkamp, J. H., and Stadhouders, A. M. (1978) *Biochem Med* **20**, 404-416
153. Byrne, E., and Trounce, I. (1985) *J Neurol Sci* **69**, 319-333
154. Hedman, R., Suranyi, E. M., Luft, R., and Ernster, L. (1962) *Biochem Biophys Res Commun* **8**, 314-320
155. Peter, J. B., and Lee, L. D. (1967) *Biochem Biophys Res Commun* **29**, 430-436
156. Rasmussen, H. N., Andersen, A. J., and Rasmussen, U. F. (1997) *Anal Biochem* **252**, 153-159
157. Rasmussen, H. N., and Rasmussen, U. F. (1997) *Mol Cell Biochem* **174**, 55-60
158. Sahlin, K., Fernstrom, M., Svensson, M., and Tonkonogi, M. (2002) *J Physiol* **541**, 569-574
159. Vallieres, J., Scarpa, A., and Somlyo, A. P. (1975) *Arch Biochem Biophys* **170**, 659-669
160. Max, S. R., Garbus, J., and Wehman, H. J. (1972) *Anal Biochem* **46**, 576-584
161. Bullock, G. R., Carter, E. E., and White, A. M. (1973) *Biochim Biophys Acta* **292**, 350-359
162. Zheng, X. X., Shoffner, J. M., Voljavec, A. S., and Wallace, D. C. (1990) *Biochim Biophys Acta* **1019**, 1-10

FOOTNOTES

*This work was supported by NIEHS 012691 (C.G.) and RC1DK087307 (C. G.) and grants 2R01 AR043140 and 1P01 AR052354 from the National Institutes of Health. We wish to thank the technical assistance of Yi-Fan Zhang (mtDNA studies), Amanda Pires (glycogen and fat content evaluations), Amy Ng (citrate synthase activity), Shimwoo Lee (Young Scholars Program; PKC signal transduction pathway), and Yasmine Parsaei (Young Scholars Program; mtDNA studies). We wish to thank Dr. Peter G. Green (Dept. Civil & Environmental Engineering; University of California Davis) for his assistance at evaluating calcium content in the samples by ICP-MS; Ms. Isela Padilla for her technical assistance with the RyR1 western blots.

The abbreviations used are: ROS, reactive oxygen species; MH, malignant hyperthermia; MHS, MH-susceptible;

MHN, MH-non susceptible; RYR1, type 1 ryanodine receptor; CCD, central core disease; T2D, type 2 diabetes.

FIGURE LEGENDS

Figure 1. **A** Representative western blot of RyR1 protein in the whole membrane fraction of skeletal muscle isolated from WT and R163C mice. RyR1 expression was detected by separating the proteins by SDS-PAGE, followed by western blotting as described under Materials and Methods. Total protein applied was 10 $\mu\text{g}/\text{lane}$. **B** Summary densitometry data of RyR1 protein in WT and R163C mice expressed in fluorescence units *per* μg protein. Densitometry was performed on at least four separate blots **C** Representative western blot of myoglobin, ATPase beta-subunit, and Complex II 70-kDa subunit in the mitochondrial and post-mitochondrial fractions from skeletal muscle obtained from WT mice. Experimental details were given under Materials and Methods.

Figure 2. Protein and transcript levels of mitochondrial proteins in skeletal muscle from R163C relative to WT. **A** Mitochondrial protein expression expressed as percentage of WT values. Western blots of the indicated mitochondrial proteins were performed on mitochondrial fractions from WT and R163C skeletal muscle. Dashed lines indicate the average of protein expression for nDNA- or mtDNA-encoded proteins. Abbreviations: SDHA, Complex II 70-kDa subunit; CCO I, cytochrome *c* oxidase subunit I; ATPB, ATPase β -subunit; VDAC-1, voltage-dependent anion channel 1; MnSOD, Mn-dependent superoxide dismutase; CCO II, cytochrome *c* oxidase subunit II; ND1 and ND6 subunits 1 and 6 of NADH dehydrogenase. **B.** The transcript level of each gene was normalized to actin, and then expressed as the fold difference to the WT values. All experimental details for RNA extraction, cDNA preparation, and PCR conditions were explained in detail under Materials and Methods. Dashed line indicates the WT values. Abbreviations: CYTB, cytochrome *b*; MRPL10, mitochondrial ribosomal protein L10. Asterisks indicate statistically significant differences when compare to their respective WT values ($p = 0.007$ and 0.01 , for CYTB and ND1, respectively).

Figure 3. Densitometry of protein bands detected by western blotting in R163C skeletal muscle. Western blots for myoglobin, calcineurin and RCAN 3 were obtained for WT and R163C skeletal muscle. The intensities of the bands were normalized to actin (used as a loading control). Western blots of pAMPK (Thr 172) and pACC (Ser 79) were normalized to each respective total and unphosphorylated protein (i.e., AMPK and ACC). Western blots for pPKC epsilon (Ser 660) and pPKC alpha (Thr 638/641) were normalized to a pan PKC and PKC alpha, respectively. All results shown in the figure were expressed as percentage of WT values. No statistical differences were observed for total PKC, AMPK, or ACC2 when normalized to actin between WT and R163C.

Figure 4. **A** Transcript levels of Myh isoforms in WT and R163C skeletal muscle. All R163C values were significantly different from WT with $p < 0.03$. **B** A direct association between oxidative capacity (evaluated as citrate synthase or succinate dehydrogenase activities as markers for mitochondria) and glycogen content has

been observed (147-150), thus glycogen content in mouse muscles with various proportions of type IIB fibers was evaluated. Glycogen content was assayed on lower hind leg muscles tibialis anterior (TA), extensor digitorum longus (EDL), soleus (SOL), gastrocnemius (GST), the upper hind leg muscle, quadriceps (QUAD), the back muscle spinalis thoracis (SPN), and brachii muscles (BRC) from female WT and R163C (brachii muscles only). The percentage of Myh4 was evaluated as described under Materials and Methods or calculated from (151) using the percentage of type IIB in the population of fibers for that particular muscle(s). The data points were fitted to a linear regression ($r^2 = 0.81$ with a $p < 0.05$ using Chi square goodness of fit). Glycogen content decreased from muscles constituted mainly of type I (or slow-twitch) fibers to those that have a higher proportion of fast-twitch fibers.

Figure 5. Scheme of the metabolism and signal transduction pathways in R163C skeletal muscle.

See explanation in the text. Bold letters indicate the parameters evaluated in this study. The scheme was based on the data obtained in this study and classified according to DAVID Functional Classification Tool (67,68).

TABLE I: Comparison of mitochondrial content, yield, and parameters from our study and those published in the literature

	WT	R163C	Literature*
Mitochondrial content of skeletal muscle ^a (mg mitochondrial protein/g tissue wet weight)	1.8 ± 0.2	1.1 ± 0.8 [†]	[0.1-5.0]
Protein yield ^b (mg mitochondrial protein/100 mg homogenate protein)	46 ± 4	44 ± 3	[12-48]
RCR	6.1 ± 0.7	1.6 ± 0.3 [†]	[1.9-10.8]
P/O	2.3 ± 0.1	2.2 ± 0.1	[1.6-3.0]

*Values obtained with rat, mouse, or human skeletal muscle by using a variety of procedures (buffered KCl-EDTA, buffered mannitol-sucrose-EDTA, or sucrose; supplemented with ATP, MgCl₂, heparin, fatty acid-free BSA, among others; mechanical cell/tissue disruption vs. enzymatic digestion; use of mitochondria purification in Percoll or sucrose gradients; (52,152-162).

^a Evaluated as the activity of citrate synthase in the mitochondrial fraction (expressed in mg mitochondrial protein) relative to the activity in whole muscle (expressed in g tissue wet weight).

^b Evaluated as the activity of citrate synthase in the mitochondrial fraction (expressed in mg mitochondrial protein) relative to the activity in whole muscle (expressed in mg tissue protein).

[†] Significantly different from WT with $p = 0.03$

TABLE II: State 3 oxygen uptake rates of skeletal muscle mitochondria from wild-type and R163C mice

	State 3 oxygen uptake rates	
	Malate-glutamate	Succinate
Wild-type	21 ± 1	34 ± 1
R163C	13.0 ± 0.4*	11 ± 1*
State 3 oxygen uptake rate normalized to citrate synthase activity		
Wild-type	5.5 ± 0.5	8.9 ± 0.8
R163C	2.2 ± 0.1*	1.9 ± 0.2*

State 3 oxygen uptake rates were evaluated in the presence of the indicated substrate and ADP and expressed as nmol oxygen consumed x (min x mg protein)⁻¹. These rates were normalized by citrate synthase activities and multiplied by 100. All R163C numbers indicated with an asterisk were significantly different from WT with $p < 0.05$.

TABLE III: *Glucose uptake and ATP produced during anaerobic and aerobic glycolysis in diaphragm from WT and R163C mice*

	WT	R163C	<i>p</i> -value	Percentage of WT
Glucose consumed*				
Total	9 ± 1	7.3 ± 0.6	0.04	81 ± 10
Anaerobic	5.52 ± 0.08	6.1 ± 0.1	0.015	111 ± 2
OXPHOS	3.35 ± 0.09	1.1 ± 0.2	0.0003	33 ± 5
ATP produced				
Total	109 ± 2	50 ± 3	0.04	46 ± 3
Anaerobic	11.0 ± 0.2	12.1 ± 0.2	0.015	110 ± 2
OXPHOS	98 ± 3	38 ± 5	0.0003	39 ± 5

The amount of glucose consumed or ATP produced in 2.5 hours was expressed as μmol glucose (or ATP)/g muscle wet weight. Glucose was determined in aliquots taken at various time points for 2.5 hours as described under Materials and Methods. To determine the amount of glucose consumed in anaerobic glycolysis, lactate was evaluated in parallel aliquots taken at the same time points as glucose and considering the stoichiometry of 2 lactate produced per glucose consumed. Glucose consumed during OXPHOS was evaluated by measuring the oligomycin-sensitive oxygen consumed by muscle in glucose-supplemented buffered Ringer solution and considering the stoichiometry of 6 oxygen *per* glucose consumed. The amount of ATP produced during OXPHOS was evaluated by using the experimental P/O ratio. The amount of ATP produced during anaerobic glycolysis was calculated by using the stoichiometry of 2 ATP/lactate produced.

TABLE IV: Mitochondrial and cytosolic calcium in skeletal muscle mitochondria from wild-type (WT) and R163C mice

	Calcium content (nmol calcium x (g tissue wet weight) ⁻¹)	
	Mitochondria	Cytosol
Wild-type mice	35 ± 3	839 ± 2
R163C mice	198 ± 2*	1512 ± 3*

Calcium content was determined by ICP-MS in each fraction.

*Significantly different from WT with $p < 0.05$.

TABLE V: Complex activities in skeletal muscle mitochondria from WT and R163C mice

Complex	Activity*		<i>p</i> -value	R163C/WT (%)
	WT	R163C		
I	11.9 ± 0.3	4 ± 2	0.004	34
II	2.7 ± 0.3	3.59 ± 0.04	0.14	133
II-III	68.1 ± 0.7	46 ± 2	0.012	68
IV	38 ± 2	19.1 ± 0.8	0.003	50
V	45 ± 2	51 ± 5	0.23	113

*All activities were expressed as nmol x (min x mg protein)⁻¹.

TABLE VI: Transcript levels of myosin heavy chain isoforms in skeletal muscle from WT and R163 mice

Myh isoform	Main component of fiber type	Contraction time	WT	R163C	<i>p</i> -value	R163/WT
<i>Myh1</i>	IIX/D	Fast twitch	1.69 ± 0.01	1.41 ± 0.02	3 x 10 ⁻⁴	0.83
<i>Myh2</i>	IIA	Fast twitch	0.89 ± 0.02	0.438 ± 0.005	3 x 10 ⁻⁵	0.49
<i>Myh4</i>	IIB	Fast twitch	13.8 ± 0.4	7.0 ± 0.3	2 x 10 ⁻⁴	0.51
<i>Myh7</i>	I	Slow twitch	0.0182 ± 0.0002	0.0053 ± 0.0004	1 x 10 ⁻⁵	0.30

TABLE VII: ROS production by skeletal muscle mitochondria

	Wild-type	R163C
Rate of H ₂ O ₂ production (nmol H ₂ O ₂ x (min mg protein) ⁻¹)	0.2	0.6*
Rate of O ₂ consumption (nmol O ₂ x (min mg protein) ⁻¹)	2.1	4.9*
Fraction of O ₂ uptake in State 4 destined to H ₂ O ₂ production (%)	9.5	12.2*

The rates of H₂O₂ production and O₂ consumption were measured in the presence of succinate, rotenone, and antimycin. The rates were linear for at least 5-6 min. Other details were indicated under Materials and Methods. The values are mean with SD ≤ 12% mean. *R163C numbers were significantly different from WT with $p < 0.05$.

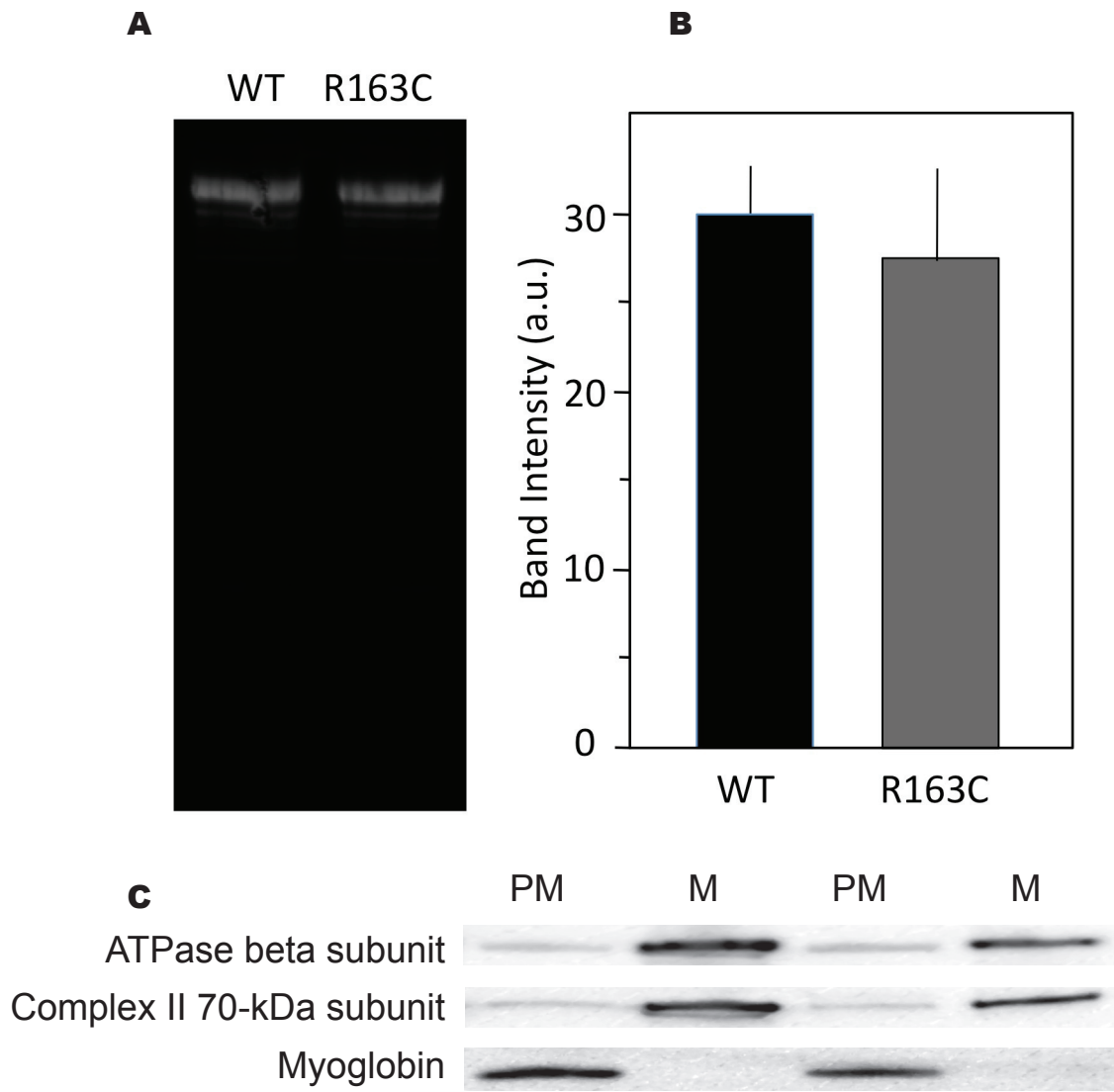


FIGURE 1

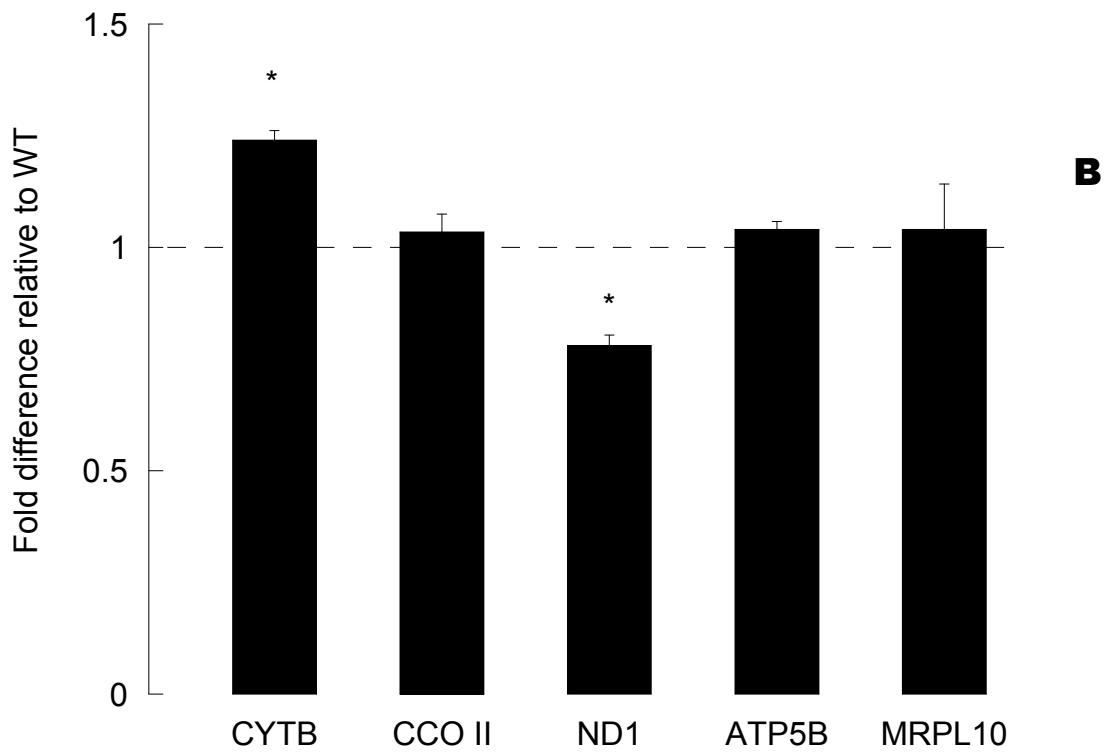
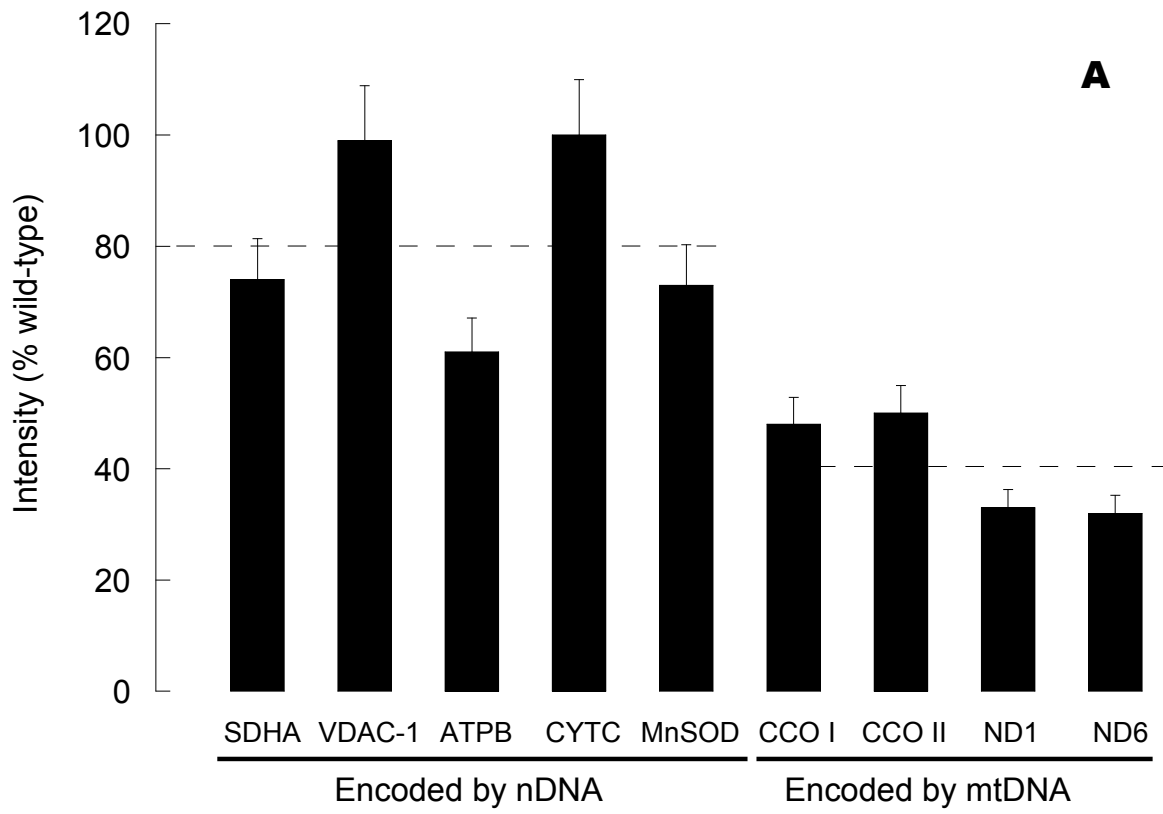


FIGURE 2

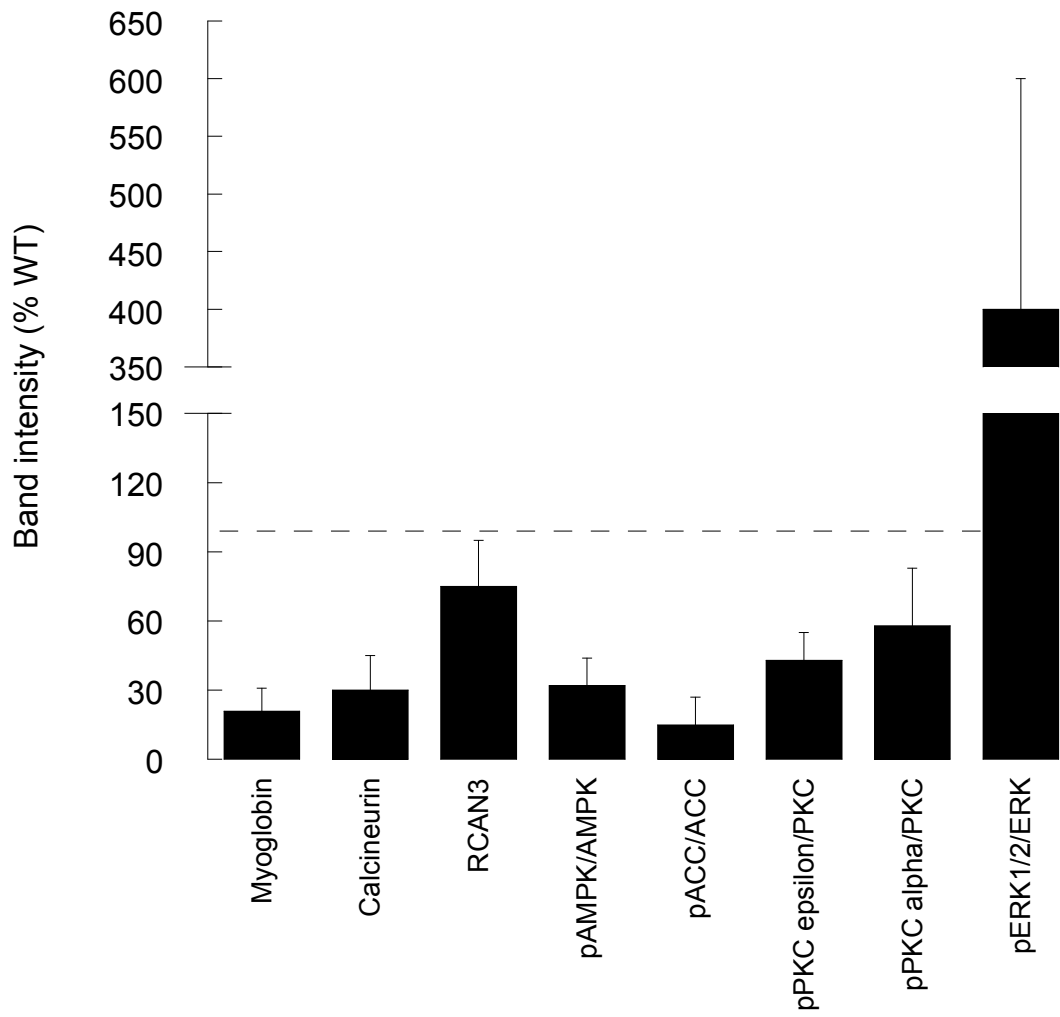


FIGURE 3

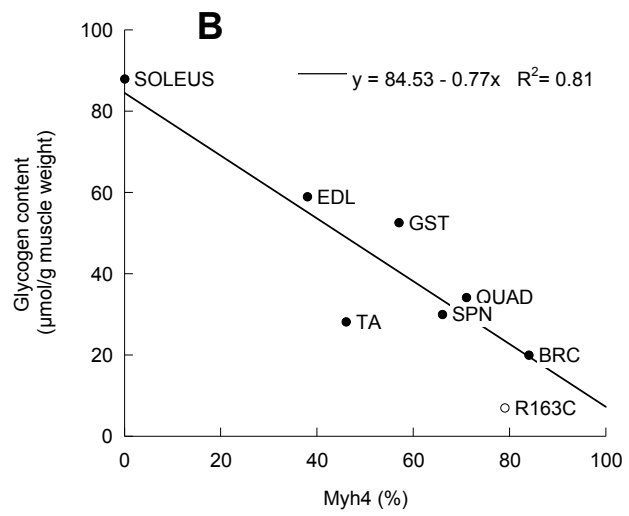
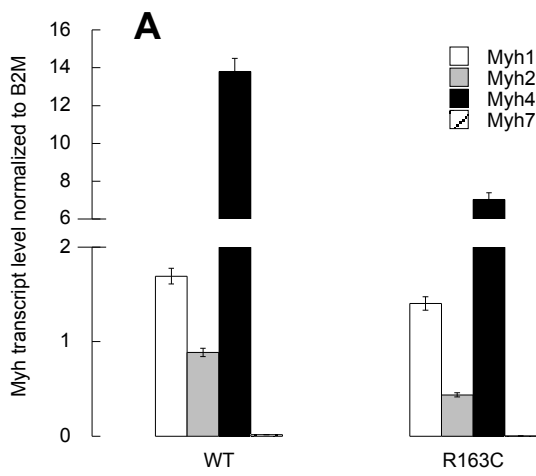


FIGURE 4

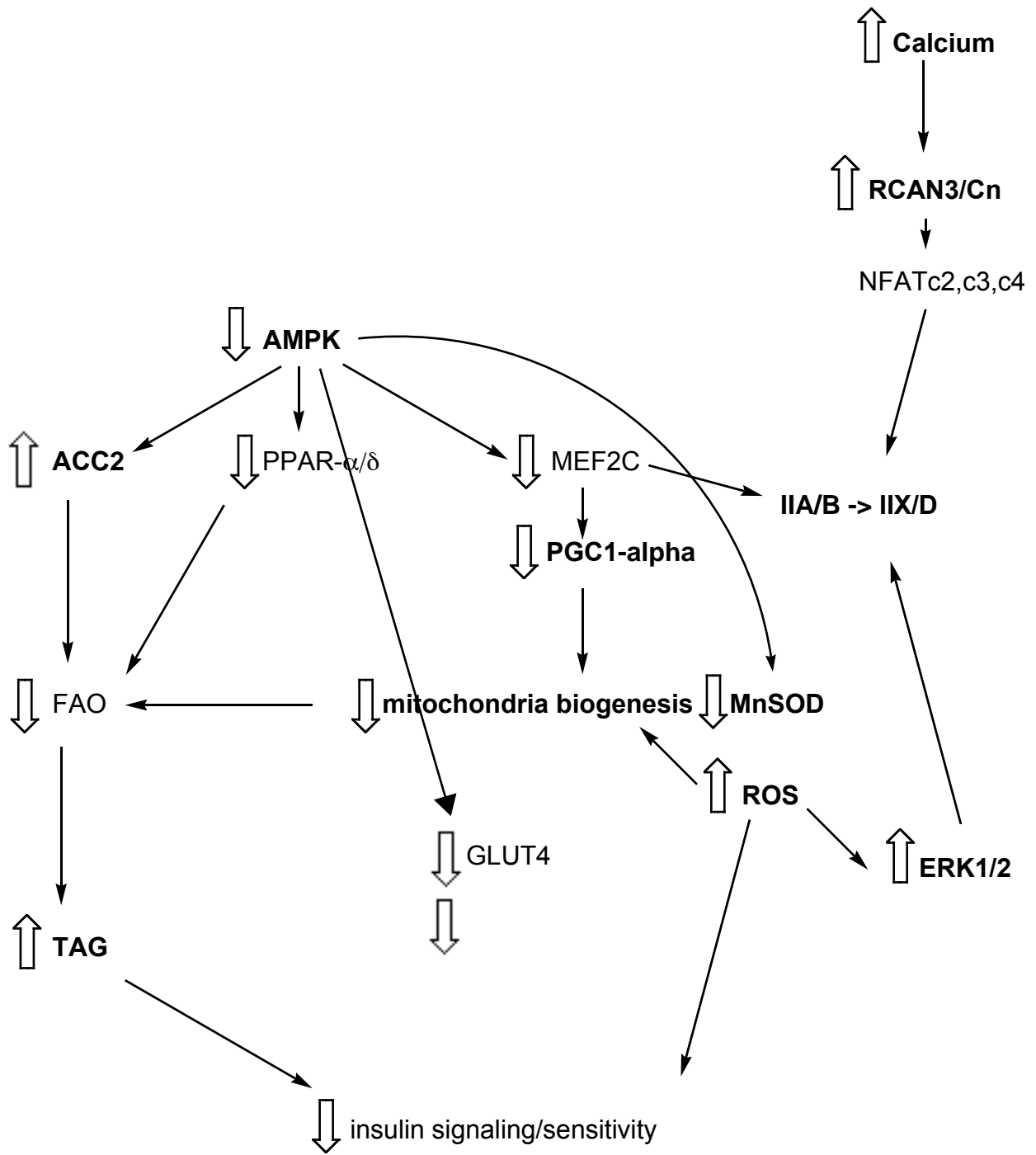


FIGURE 5